Arf6 regulates AP-1B–dependent sorting in polarized epithelial cells

Elina Shteyn, Lucy Pigati, and Heike Fölsch

Department of Cell and Molecular Biology, Northwestern University, Chicago, IL 60611

The epithelial cell–specific clathrin adaptor complex AP-1B facilitates the sorting of various transmembrane proteins from recycling endosomes (REs) to the basolateral plasma membrane. Despite AP-1B's clear importance in polarized epithelial cells, we still do not fully understand how AP-1B orchestrates basolateral targeting. Here we identify the ADP-ribosylation factor 6 (Arf6) as an important regulator of AP-1B. We show that activated Arf6 pulled down AP-1B in vitro. Furthermore, interfering with Arf6 function through overexpression of dominant-active Arf6Q67L or dominant-negative Arf6D125N, as well as depletion of Arf6 with short hairpin RNA (shRNA), led to apical missorting of AP-1B–dependent cargos. In agreement with these data, we found that Arf6 colocalized with AP-1B and transferrin receptor (TfnR) in REs. In addition, we observed specific recruitment of AP-1B into Arf6-induced membrane ruffles in nonpolarized cells. We conclude that activated Arf6 directs membrane recruitment of AP-1B, thus regulating AP-1B's functions in polarized epithelial cells.

Introduction

Epithelial cells polarize their plasma membrane into apical and basolateral domains to facilitate vectorial transport of nutrients and waste products (Martin-Belmonte and Mostov, 2008). To maintain this apical-basolateral polarity, epithelial cells sort newly synthesized and recycling transmembrane proteins either in the TGN, recycling endosomes (REs), or both according to their final destination (Mellman and Nelson, 2008; Fölsch et al., 2009).

Sorting to the basolateral membrane frequently depends on a short peptide motif (YxxØ) encoded in the cytoplasmic tail of the transmembrane protein, which is recognized by heterotetrameric clathrin adaptor protein complexes (Rodriguez-Boulan et al., 2005). There are four major classes: AP-1 through AP-4 (Boehm and Bonifacino, 2001; Brodsky et al., 2001). Whereas AP-2 localizes to the plasma membrane and facilitates clathrin-mediated endocytosis, AP-1, AP-3, and AP-4 localize to endomembranes and sort cargo in the biosynthetic and/or endocytic pathways (Nakatsu and Ohno, 2003). Epithelial cells have two AP-1 complexes—AP-1A and AP-1B—which share the two large subunits (γ- and β1-adaptin) and the small subunit (σ1-adaptin), but differ in the incorporation of the medium subunits μ1A or the epithelial cell–specific μ1B (Fölsch, 2005). Although μ1A and μ1B are 79% identical on the amino acid level (Ohno et al., 1999), AP-1A and AP-1B localize to different intracellular compartments and carry out different functions (Fölsch et al., 1999, 2001, 2003). AP-1A localizes to the TGN and/or early endosomes and is involved in endosomal/lysosomal targeting. TGN localization of AP-1A is achieved through interaction of AP-1A with the TGN-enriched lipid phosphatidylinositol 4-phosphate (PI[4]P) and Arf1 (Hirst and Robinson, 1998; Wang et al., 2003). In contrast, AP-1B localizes in REs and facilitates sorting of biosynthetic and endocytic cargos to the basolateral plasma membrane (Fölsch, 2005). Biosynthetic cargos that use AP-1B on their way to the surface first move from the TGN into REs in a pathway that is regulated by Rab13 (Ang et al., 2004; Nokes et al., 2008). Examples of cargos that follow this pathway are the vesicular stomatitis virus glycoprotein (VSVG) and truncated low-density lipoprotein receptors (LDLR-CT27; Fields et al., 2007; Nokes et al., 2008). Recently, we identified phosphatidylinositol 3,4,5-trisphosphate (PI[3,4,5]P_3) as a signature lipid in REs of AP-1B–positive epithelial cells, and PI(3,4,5)P_3 was necessary for AP-1B recruitment (Fields et al., 2010). However, because polarized epithelial cells also exhibit PI(3,4,5)P_3 accumulation

Correspondence to Heike Fölsch: h-folsch@northwestern.edu

Abbreviations used in this paper: CHX, cycloheximide; GAPDH, glyceraldehyde 3-phosphate dehydrogenase; GEF, guanine nucleotide exchange factor; PH, pleckstrin homology; PI(3,4,5)P_3, phosphatidylinositol 3,4,5-trisphosphate; PIPK, phosphatidylinositol 4-phosphate 5-kinase; PLD, phospholipase D; RE, recycling endosome; shRNA, short hairpin RNA; TfnR, transferrin receptor; VSVG, vesicular stomatitis virus glycoprotein.

The Rockefeller University Press $30.00
J. Cell Biol. Vol. 194 No. 6 873–887
www.jcb.org/cgi/doi/10.1083/jcb.201106010

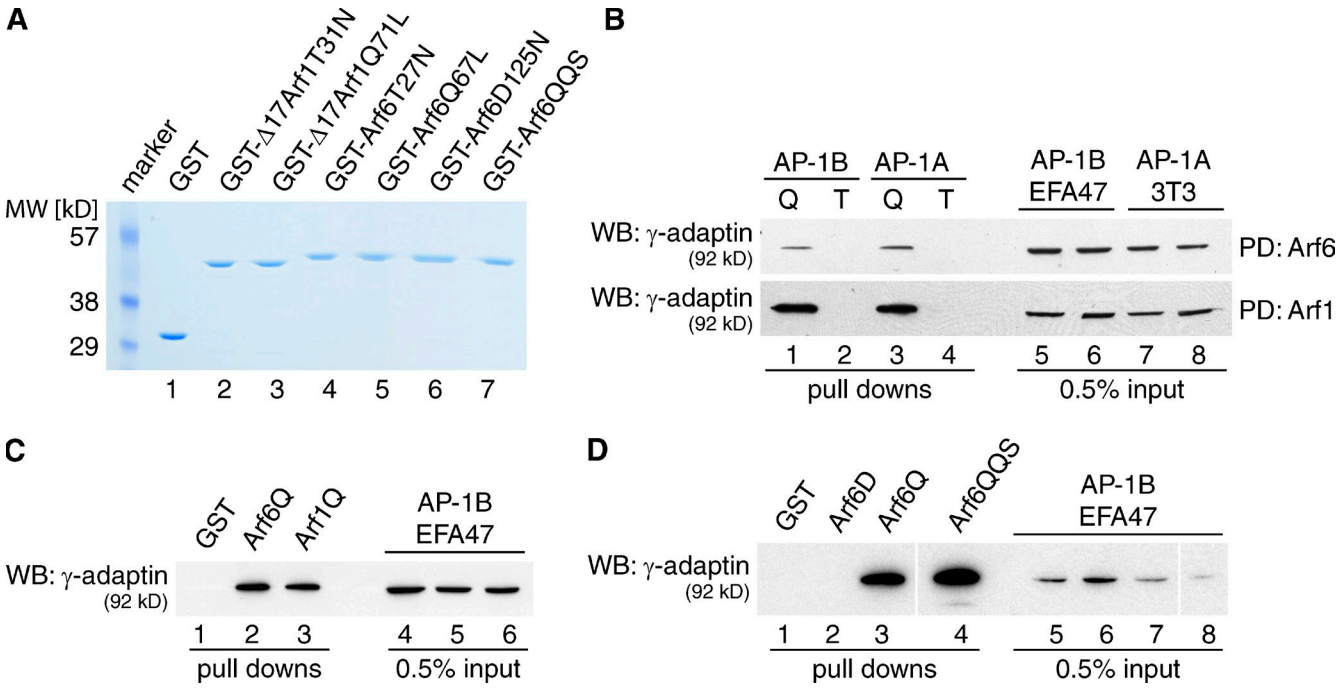

Figure 1. **Arf6 pulls down AP-1B in vitro.** (A) 1 µg of purified proteins were run on an SDS gel and stained with Coomassie dye. Arf6QQS, Arf6Q67L/Q37E/S38I. (B) EFA47 or 3T3 cell lysates were incubated with GST-Arf6Q67L (Q, lanes 1 and 3) or GST-Arf6T27N (T, lanes 2 and 4; top), and GST-Δ17Arf1Q71L (Q, lanes 1 and 3) or GST-Δ17Arf1T31N (T, lanes 2 and 4; bottom). 0.5% input material for lanes 1–4 is shown in lanes 5–8, respectively. PD, pull down. (C) EFA47 cell lysate was incubated with GST (lane 1), GST-Arf6Q67L (Arf6Q, lane 2), or GST-Δ17Arf1Q71L (Arf1Q, lane 3). 0.5% input material for lanes 1–3 is shown in lanes 4–6, respectively. (D) EFA47 cell lysate was incubated with GST (lane 1), GST-Arf6D125N (Arf6D, lane 2), GST-Arf6Q67L (Arf6Q, lane 3), or GST-Arf6Q67L/Q37E/S38I (Arf6QQS, lane 4). 0.5% input material for lanes 1–4 is shown in lanes 5–8, respectively. Note, all lanes shown in D were run on the same gel and processed together. The two white lines indicate where the scanned data were cropped together to remove unrelated lanes (i.e., between lanes 3 and 4, and 7 and 8). (B–D) Samples were processed as described in Materials and methods. Western blots (WB) were decorated with antibodies directed against γ-adaptin.

at the basolateral plasma membrane (Gassama-Diagne et al., 2006), PI(3,4,5)P_3 alone cannot be sufficient for specific membrane recruitment of AP-1B, and other factors must aid in defining AP-1B's intracellular localization.

Arf6 is the sole member of the class III Arf proteins, and is known for its function in clathrin-mediated endocytosis, endocytic recycling, and cell migration (Donaldson, 2003; D'Souza-Schorey and Chavrier, 2006). To fulfill its different tasks, Arf6 interacts with a variety of effector proteins. For example, Arf6 interacts with and stimulates phospholipase D (PLD), an enzyme that cleaves phosphatidylcholine to generate phosphatidic acid (Vitale et al., 2005). Activation of PLD by Arf6 is necessary for recycling of endocytic cargo in µ1B-negative HeLa cells (Jovanovic et al., 2006). Moreover, Arf6 regulates the actin cytoskeleton, perhaps through interactions with its guanine nucleotide exchange factor (GEF) EFA6 (Luton et al., 2004). In addition, Arf6 interacts with phosphatidylinositol 4-phosphate 5-kinase Iγ-90 (PIPKIγ-90), which is important for phosphatidylinositol 4,5-bisphosphate (PI[4,5]P_2) production during AP-2–dependent endocytosis (Krauss et al., 2003). Interestingly, PIPKIγ-90 also interacts with AP-1B (Ling et al., 2007) and has been suggested to play a role in PI(3,4,5)P_3 formation in REs (Fields et al., 2010). In epithelial cells, it has further been suggested that Arf6 operates in REs, where it may directly interact with and recruit the Sec10 subunit of the exocyst complex (Prigent et al., 2003) independently or in cooperation with AP-1B (Fölsch et al., 2003). The exocyst complex is believed to tether AP-1B vesicles to the sites of fusion at the basolateral membrane (Fölsch, 2005). It should be noted, however, that direct evidence of Arf6 localization in REs is missing so far. In contrast, early studies with µ1B-negative CHO cell lysates suggested that Arf6 might exclusively localize to the plasma membrane (Cavenagh et al., 1996).

In this study, we define a novel role for Arf6 in basolateral exocytosis from REs via regulation of the AP-1B pathway.

Results

Arf6 interacts with AP-1B in vitro

First we tested whether AP-1B might interact with the two major Arf proteins present in cells: Arf1 and Arf6. Although the function of Arf1 in coat recruitment is well documented (D'Souza-Schorey and Chavrier, 2006), the involvement of Arf6 in direct coat recruitment is less clear. However, there have been some studies indicating that Arf6 may directly interact with adaptor proteins. Arf6 could be cross-linked to AP-1A and AP-3 (Austin et al., 2002), and activated Arf6 could precipitate AP-1A from brain lysate (Krauss et al., 2003). To test whether Arf1 or Arf6 may interact with AP-1B, we created fusion proteins of GST and various Arfs. We first tested the dominant-active mutants Arf1Q71L and Arf6Q67L as well as the dominant-negative mutants Arf1T31N and Arf6T27N. Arf1Q71L and Arf6Q67L can no longer hydrolyze GTP and are thus locked in the GTP forms, whereas Arf1T31N and Arf6T27N are locked

in the GDP forms (Donaldson, 2003; Nie and Randazzo, 2006). Furthermore, in this assay, we used Arf1 proteins with deleted N termini, Δ17Arf1Q71L and Δ17Arf1T31N, to ensure functionality (Paris et al., 1997).

GST fusion proteins were purified from *Escherichia coli* (Fig. 1 A). Subsequently, purified proteins were bound to glutathione beads and incubated with cell lysate of EFA47 cells as a probe for AP-1B or lysate of 3T3 fibroblasts as a probe for AP-1A as a positive control. EFA47 cells are mouse embryonic fibroblasts that are knocked out for μ1A/AP-1A, but express μ1B/AP-1B exogenously (Fölsch et al., 2001; Eskelinen et al., 2002). We found that both active mutant proteins, Arf6Q67L and Arf1Q71L, pulled down AP-1B and AP-1A (Fig. 1 B), whereas the inactive Arf6T27N and Arf1T31N mutant proteins did not pull down either adaptor complex (Fig. 1 B). In a direct comparison, activated Arf6 and activated Arf1 pulled down comparable amounts of AP-1B (Fig. 1 C). Furthermore, AP-1B was also precipitated by an Arf6 effector domain mutant, Arf6Q67L/Q37E/S38I, but not by the inactive mutant protein Arf6D125N (Fig. 1 D).

In conclusion, it is possible that either Arf1 or Arf6 may play a role in recruiting AP-1B onto membranes.

Arf6Q67L leads to apical missorting of VSVG

To test the idea that Arf1 or Arf6 may play a role in basolateral sorting, we used a microinjection-based assay in which cDNAs encoding V5-tagged Arf mutant proteins were injected into polarized, filter-grown MDCK cells (Cook et al., 2011). As shown previously, this assay of acute overexpression typically prevents the onset of secondary effects often observed with long-term overexpression of mutant GTPases by transient transfections (Nokes et al., 2008).

First we analyzed VSVG sorting in the presence of overexpressed Arf6 mutant proteins. We coinjected cDNAs encoding Arf6T27N or Arf6Q67L together with plasmids encoding the temperature-sensitive, GFP-tagged VSVGts045. The VSVGts045-GFP variant used here has an added spacer (SP) between the cytoplasmic tail and the GFP moiety to allow for efficient basolateral sorting (Keller et al., 2001). Using VSVGts045 has the added benefit that surface delivery can be arrested in the ER at the nonpermissive temperature of 39°C while the mutant Arf6 proteins are synthesized in the cytosol. After 2 h of incubation at 39°C, cells were shifted to the permissive temperature of 31°C for 2 h in the presence of cycloheximide (CHX) to prevent further protein synthesis. At 31°C, VSVGts045-GFP folds correctly and is delivered to the plasma membrane (Scales et al., 1997). During surface delivery, VSVG moves from the TGN into REs to be sorted along the AP-1B pathway (Fölsch et al., 2003; Ang et al., 2004). VSVG at the surface was stained with an antibody recognizing its ectodomain before fixation and staining for V5-tagged Arf6. Specimens were analyzed by confocal microscopy and quantified using Volocity software to determine the percentage of total VSVG pixels at the basolateral membrane, as described in Materials and methods. We found that in both mock-injected cells and cells coexpressing

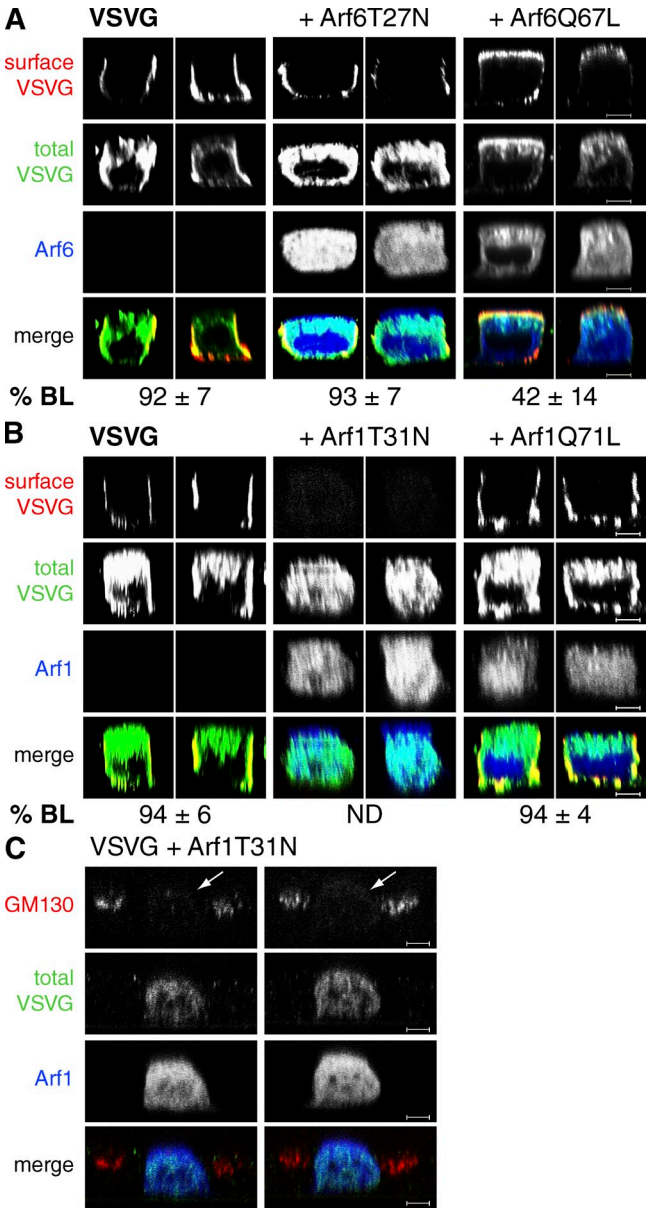

Figure 2. **Arf6Q67L leads to apical missorting of VSVG.** MDCK cells grown on filter supports for 3 d were microinjected with plasmids encoding VSVGts045-GFP at 39°C in combination with V5-tagged Arf6T27N or V5-tagged Arf6Q67L (A), or together with V5-tagged Arf1T31N (B and C) or V5-tagged Arf1Q71L (B). Cells were then incubated for 2 h at 39°C followed by 2 h at 31°C in the presence of CHX. Subsequently, cells were stained for V5-tagged Arf proteins, total VSVG (anti-GFP antibodies), and surface VSVG (A and B), or Arf1T31N-V5 and endogenous GM130 (C). Specimens were analyzed by confocal microscopy and representative xz sections are shown. Arrows in C denote microinjected cells. Data in A and B represent mean values and SD of pixel distributions determined from at least three independent experiments as described in Materials and methods. For A, we analyzed 34 mock-injected cells, 35 cells coexpressing Arf6T27N, and 33 cells coexpressing Arf6Q67L. $P < 0.0001$ for Arf6Q67L compared with the mock control. For B, we analyzed 39 mock-injected cells and 44 cells coexpressing Arf1Q71L. ND, not determined. Bars, 5 μm.

Arf6T27N, VSVG was efficiently delivered to the basolateral membrane (92% and 93%, respectively; Fig. 2 A). In contrast, we found only 42% of the total VSVG at the basolateral membrane in cells coexpressing Arf6Q67L (Fig. 2 A, $P < 0.0001$,

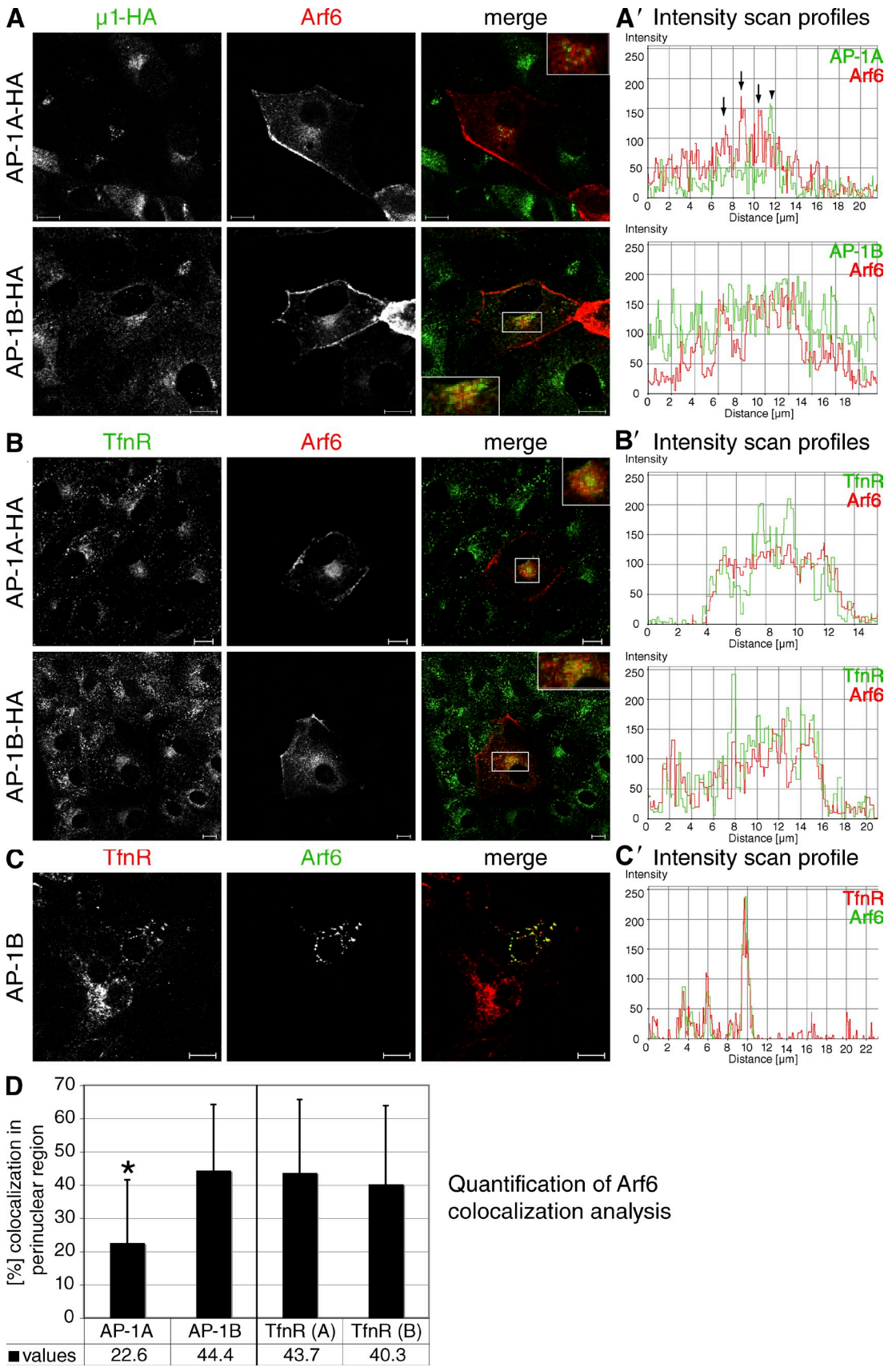

Figure 3. **Arf6 partially colocalizes with AP-1B in REs.** (A and B) LLC-PK1 cells stably expressing μ1A-HA or μ1B-HA were seeded onto coverslips. 2 d after seeding, cells were transfected with plasmids encoding V5-tagged wild-type Arf6. After 21–22 h, cells were fixed and stained for Arf6-V5 and μ1A-HA or μ1B-HA (A), or TfnR (B). Specimens were analyzed by confocal microscopy and representative images are shown. Insets are 2× magnifications of boxed areas. A′ and B′ show fluorescence intensity profiles through a region in the boxed area for Arf6 and AP-1A, AP-1B, or TfnR. Noncoincidental

see figure legend). Importantly, Arf6Q67L did not disrupt polarity in general, as judged by the lateral staining of the marker protein gp58, the tight junction localization of ZO-1, and the presence of the primary cilium under the same experimental conditions (Fig. S1, A and B, middle panels).

We then tested Arf1T31N and Arf1Q71L in the same assay. Unlike Arf6Q67L, overexpression of Arf1Q71L had no effect on basolateral delivery of VSVG (Fig. 2 B). Because both Arf1Q71L and Arf6Q67L are able to pull down AP-1B to the same extent in vitro (Fig. 1 C), these results argue that Arf6Q67L may not simply titer out AP-1B in the cytosol but may inhibit basolateral sorting through a more specific mechanism. Furthermore, we observed a complete inhibition of surface delivery in the presence of Arf1T31N (Fig. 2 B). This is most likely caused by a loss of functional Golgi, as indicated by a lack of GM130 staining in virtually every microinjected cell analyzed (Fig. 2 C). A similar effect is seen after adding the fungal metabolite brefeldin A to eukaryotic cells, which inhibits the Golgi-localized Arf1 GEFs BIG1, BIG2, and GBF1 and results in a secretion block from the ER (Klausner et al., 1992; Citterio et al., 2008).

To summarize, direct comparison of Arf1 and Arf6 mutant proteins in a microinjection-based sorting assay suggests that Arf6 but not Arf1 may have a regulatory function in the AP-1B pathway.

Arf6 partially colocalizes with AP-1B in REs

Because Arf proteins typically localize to donor membranes to facilitate vesicle formation (D'Souza-Schorey and Chavrier, 2006), we sought to localize Arf6 in epithelial cells. To this end we used LLC-PK1 cell lines stably expressing µ1A or µ1B with internal HA tags (LLC-PK1::µ1A-HA or LLC-PK1::µ1B-HA; Fölsch et al., 2003). Because of the lack of an antibody suitable for Arf6 detection by immunofluorescence, we transiently expressed low levels of V5-tagged wild-type Arf6 in cells grown in large clusters on coverslips and costained for Arf6 and AP-1A or AP-1B. Specimens were analyzed by confocal microscopy. We then determined the percentage overlap between Arf6 and AP-1A or AP-1B at the TGN or in REs, respectively, using Volocity software as described in Materials and methods. We found only a small percentage (23%) of exogenously expressed Arf6 colocalizing with AP-1A at the TGN (Fig. 3, A, A′, and D). In contrast, Arf6 showed a significantly ($P < 0.001$) higher degree of colocalization with AP-1B in REs (44%) in addition to its localization at the plasma membrane (Fig. 3, A, A′, and D).

To confirm the recycling endosomal localization of Arf6, we then analyzed Arf6 staining relative to that of transferrin receptor (TfnR). Perinuclear TfnR staining is commonly used as a marker for REs (Sheff et al., 1999). We found partial colocalization between Arf6 and TfnR in both LLC-PK1::µ1A-HA (44%) and LLC-PK1::µ1B-HA (40%) cells (Fig. 3 B, B′, and D). To analyze whether the observed localization of Arf6 in REs is also present in polarized cells, we grew LLC-PK1 cells stably transfected with µ1B (LLC-PK1::µ1B) on filter supports, transiently transfected polarized cells with plasmids encoding V5-tagged Arf6, and analyzed Arf6 localization with respect to TfnR. We found Arf6 and TfnR colocalizing in REs of polarized cells (Fig. 3, C and C′).

Thus, in epithelial cells, Arf6 localizes to the plasma membrane and localizes partially in REs together with AP-1B and TfnR.

VSVG sorting in the presence of various Arf6 mutant proteins

To learn more about the function of Arf6 in AP-1B–dependent sorting, we created various Arf6 mutant alleles as described in the literature and analyzed their effects on VSVGts045-GFP sorting using overexpression of V5-tagged Arf6 mutant proteins by microinjection as an assay.

First, we introduced an effector domain mutation into Arf6 to create Arf6N48I. This mutant still binds to PLD, but is deficient in PLD activation and inhibits Arf6 signaling through PLD (Vitale et al., 2005; Jovanovic et al., 2006). Because we introduced the N48I mutation into wild-type Arf6, we first tested the fidelity of VSVG sorting in the presence of overexpressed Arf6. As shown in Fig. 4, VSVG was still largely basolateral (87%) in the presence of Arf6. The same was true for VSVG sorting in the presence of Arf6N48I (86% basolateral). Thus it seems that activation of PLD through Arf6 may not be a necessary function in basolateral sorting.

Next we mutated two residues adjacent to the switch I domain—Q37 and S38—in Arf6Q67L to create the effector domain mutant Arf6Q67L/Q37E/S38I. This mutant is defective in remodeling the actin cytoskeleton (Al-Awar et al., 2000; Palacios et al., 2001) without inhibiting Arf6-mediated membrane trafficking steps (Al-Awar et al., 2000; Palacios et al., 2001). Moreover, Arf6Q67L/Q37E/S38I precipitated AP-1B as well as Arf6Q67L in vitro (Fig. 1 D, lanes 3 and 4). Because previous studies had shown that the additional Q37E/S38I mutations rescued Arf6Q67L phenotypes that were related to Arf6's function in remodeling the actin cytoskeleton (Palacios et al., 2001), we asked whether VSVG missorting was affected by these additional mutations. We observed a slight, albeit significant increase ($P < 0.0001$) in basolaterally localized VSVG (57%, Fig. 4) when Arf6Q67L/Q37E/S38I was expressed in comparison to Arf6Q67L (42%, Fig. 2 A). Because VSVG was still sorted randomly (P vs. mock control < 0.0001) it seems that actin remodeling by Arf6 may not be its primary role in basolateral targeting.

peaks are marked by arrows (Arf6) or arrowheads (AP-1A). (C) LLC-PK1 cells stably expressing µ1B were seeded onto filter supports. 3 d after seeding, cells were transfected with plasmids encoding Arf6-V5. 21–22 h after transfection, cells were fixed and stained for Arf6-V5 and endogenous TfnR. Shown is a representative focal plane with recycling endosomal staining of TfnR. Note that not all cells have this concentration of TfnR in the same focal plane. C′ shows a fluorescence intensity profile through representative endosomes in the shown focal plane. Bars, 10 µm. (D) The percent overlap between Arf6 and AP-1A-HA ($n = 20$), AP-1B-HA ($n = 24$), or TfnR in LLC-PK1::µ1A-HA (TfnR[A], $n = 30$) or LLC-PK1::µ1B-HA cells (TfnR[B], $n = 14$) was determined from at least three independent experiments using Volocity software, as described in Materials and methods. Error bars indicate SD. *, $P < 0.001$.

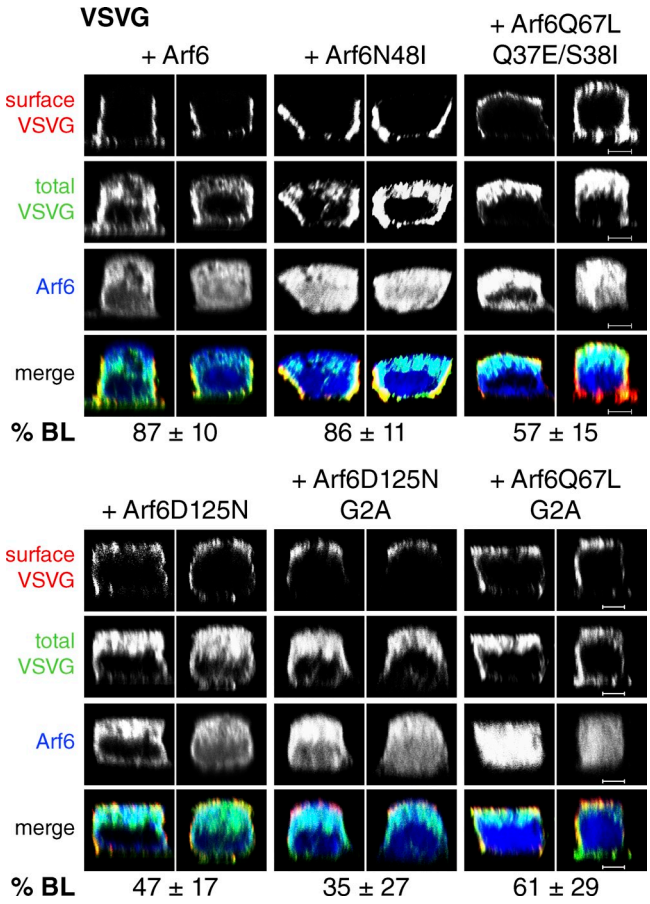

Figure 4. **Analysis of VSVG sorting in the presence of various Arf6 mutant proteins.** Polarized, filter-grown MDCK cells were coinjected with plasmids encoding VSVGts045-GFP and V5-tagged Arf6 proteins: wild-type Arf6, Arf6N48I, Arf6Q67L/Q37E/S38I, Arf6D125N, Arf6D125N/G2A, or Arf6Q67L/G2A. Cells were processed as described for VSVG (Fig. 2). Specimens were analyzed by confocal microscopy, and representative xz sections are shown. Numerical data were obtained by using Volocity software, as described in Materials and methods, from at least three independent experiments. For all conditions, numerical data for the mock control were the same as in Fig. 2 A. P-values are in comparison to the mock control unless stated otherwise. Errors indicate SD. Arf6: $n = 29$, $P = 0.0234$. Arf6N48I: $n = 39$, $P = 0.0079$. Arf6Q67L/Q37E/S38I: $n = 31$, $P < 0.0001$ in comparison to both Arf6Q67L and mock control. Arf6D125N: $n = 35$, $P < 0.0001$. Arf6D125N/G2A: $n = 35$, $P < 0.0001$ and 0.0294 in comparison to mock control and Arf6D125N, respectively. Arf6Q67L/G2A: $n = 29$, $P < 0.0001$ and 0.0014 in comparison to mock control and Arf6Q67L, respectively. Bars, 5 µm.

We then sought to test another dominant-negative allele, Arf6D125N. This protein is a nucleotide switch mutant that can no longer bind guanine nucleotides, but uses xanthine nucleotides instead (Yang and Mueckler, 1999). Thus Arf6D125N is presumed to be in an inactive, nucleotide-free form in cells. Indeed, in a GST pull-down assay, this mutant failed to precipitate AP-1B (Fig. 1 D, lane 2). We found that Arf6D125N overexpression randomized VSVG localization with only ∼50% of the total VSVG at the basolateral membrane in cells coexpressing Arf6D125N and VSVG ($P < 0.0001$, Fig. 4). This missorting was not caused by a general loss of cell polarity. As shown in Fig. S1 (A and B, right panels), the basolateral localization of gp58, the tight junction localization of ZO-1, and the presence of the primary cilium were unchanged when Arf6D125N was overexpressed after microinjection of its cDNA.

Arf6 largely resides on membranes in its GDP- and GTP-bound forms (D'Souza-Schorey et al., 1998). Thus, we sought to test whether the dominant-negative effects of Arf6D125N and Arf6Q67L were dependent on membrane localization. We introduced G2A mutations in the myristoylation motif that had been shown to result in nonmyristoylated Arf6 with a cytosolic distribution (Knorr et al., 2000). We found that a secondary G2A mutation in Arf6D125N, Arf6D125N/G2A, resulted in a statistically significant reduction of basolaterally localized VSVG from 47% down to 35% ($P < 0.03$, Fig. 4). These data indicate that Arf6D125N may be a more potent inhibitor when localized in the cytosol, perhaps because of increased interactions with its GEFs. In contrast, nonmyristoylated Arf6Q67L, Arf6Q67L/G2A, was significantly less potent ($P < 0.002$) as an inhibitor of VSVG sorting (61% basolateral, Fig. 4) than the single Arf6Q67L mutant protein (42% basolateral, Fig. 2 A). We conclude that Arf6Q67L is most active in interfering with basolateral sorting when the protein is membrane localized.

As summarized in Table I, of all Arf6 mutant proteins tested we found two single mutants that led to apical missorting of VSVG: the dominant-active Arf6Q67L and the dominant-negative Arf6D125N. Furthermore, through the use of effector domain mutant proteins, we conclude that Arf6's primary role in basolateral sorting may not be to activate PLD or to rearrange the actin cytoskeleton. Therefore, we will focus on Arf6Q67L and Arf6D125N for the remainder of the manuscript.

Arf6D125N or Arf6Q67L expression influences PI(3,4,5)P_3 levels in REs

Previously we showed that recruitment of AP-1B to REs depended on PI(3,4,5)P_3 (Fields et al., 2010). Its production may involve PI(4,5)P_2 as an intermediate and activation of PIPKIγ-90 via AP-1B (Fields et al., 2010). Because active Arf6 interacts with and stimulates the kinase activity of PIPKIγ-90 (Krauss et al., 2003), we asked whether expression of Arf6D125N or Arf6Q67L may alter PI(3,4,5)P_3 accumulation in REs. Thus, we cotransfected MDCK cells with plasmids encoding the GFP-tagged pleckstrin homology (PH) domain of Akt, PH-Akt-GFP, as a sensor for PI(3,4,5)P_3, as described previously (Fields et al., 2010), and either V5-tagged Arf6D125N or V5-tagged Arf6Q67L. Data analysis revealed ∼60% overlap between TfnR and PH-Akt-GFP in REs of control cells (Fig. S2, A, A′, and B). In contrast, overexpression of Arf6D125N or Arf6Q67L reduced the overlap between TfnR and PH-Akt-GFP in REs to ∼35% ($P < 0.0001$) or ∼45% ($P < 0.01$), respectively (Fig. S2, A, A′, and B). Furthermore, although we found ∼65% of the total PH-Akt-GFP signal at the plasma membrane in control cells, this value dropped to ∼50% ($P < 0.01$) in cells coexpressing Arf6D125N and ∼30% ($P < 0.0001$) in cells coexpressing Arf6Q67L (Fig. S2 C).

Collectively, we found a small yet significant reduction in PI(3,4,5)P_3 accumulation in REs when Arf6D125N or

Table I. **Characteristics of Arf6 mutant proteins**

Arf6 mutant protein	Phenotype	Citation	VSVG sorting[a]
Arf6Q67L	Locked in GTP form	Donaldson, 2003	Apical
Arf6D125N	Binds xanthine nucleotides, presumed nucleotide-free in cells	Yang and Mueckler, 1999	Apical
Arf6T27N	Locked in GDP form	Macia et al., 2004	Basolateral
Arf6N48I	Deficient in PLD activation	Vitale et al., 2005; Jovanovic et al., 2006	Basolateral
Arf6Q67L/Q37E/S38I	Defective in actin remodeling	Al-Awar et al., 2000; Palacios et al., 2001	Apical
Arf6G2A	Can no longer be myristoylated	Knorr et al., 2000	ND
Arf6D125N/G2A	Presumed nucleotide-free, not myristoylated	This paper	Apical
Arf6Q67L/G2A	Locked in GTP form, not myristoylated	This paper	Apical

[a]The VSVG sorting phenotypes in the presence of Arf6 mutant proteins were all obtained in this study.

Arf6Q67L were overexpressed in MDCK cells. However, because PI(3,4,5)P_3 levels did not change dramatically, this effect may not be a major reason for VSVG missorting in the presence of Arf6D125N or Arf6Q67L.

Arf6D125N fails to colocalize with AP-1B

Next we studied the localization of Arf6D125N in LLC-PK1::μ1A-HA and LLC-PK1::μ1B-HA cell lines. We transiently expressed low levels of V5-tagged Arf6D125N and costained for Arf6D125N and AP-1A-HA or AP-1B-HA. We found Arf6D125N localizing to the plasma membrane and also in a perinuclear region. Although the percent overlap between Arf6D125N and AP-1A was roughly the same (32%, Fig. 5, A, A′, and D) as the one between Arf6 and AP-1A (23%, Fig. 3 A), we observed a statistically significant change in colocalization with regards to AP-1B (Fig. 5 A, A′, and D). Unlike wild-type Arf6 (45%, Fig. 3 A), Arf6D125N failed to partially colocalize with AP-1B, and the overlap was reduced to 19% ($P < 0.0001$). Importantly, Arf6D125N still partially colocalized with TfnR in REs (45% in LLC-PK1::μ1A-HA cells and 45% in LLC-PK1::μ1B-HA cells, Fig. 5 B, B′, and D). Moreover, Arf6D125N also partially colocalized with TfnR in polarized LLC-PK1::μ1B cells (Fig. 5, C and C′).

In conclusion, the partial colocalization of Arf6D125N with the AP-1B–dependent cargo TfnR (Fölsch et al., 1999), but not with the coat complex AP-1B, in REs implies that perhaps Arf6D125N might be interfering with vesicle assembly.

Arf6D125N overexpression leads to selective missorting of AP-1B–dependent cargos

So far we found that Arf6D125N and Arf6Q67L overexpression led to apical missorting of VSVG. To test whether this effect was specific for the AP-1B pathway, we expressed additional, well-established cargos for basolateral or apical sorting using similar microinjection protocols (see the legend for Fig. 6). First we analyzed LDLR-CT27, which like VSVG moves from the TGN into REs during biosynthetic delivery (i.e., during the chase period of our protocol) to be sorted to the basolateral membrane by AP-1B in cooperation with autosomal recessive hypercholesterolemia protein (ARH; Fields et al., 2007; Kang and Fölsch, 2011). We found that on average 82% of LDLR-CT27 was delivered to the basolateral membrane in mock-injected cells. In contrast, LDLR-CT27 was missorted to the apical membrane in cells coexpressing Arf6D125N or Arf6Q67L (Fig. 6 A). In both cases, only 45% ($P < 0.0001$) of the total surface signal was left at the basolateral membrane.

We then analyzed a point mutant of LDLR, LDLR(Y18A). This cargo is thought to move from the TGN to the basolateral membrane without traversing REs during biosynthetic delivery, and basolateral localization is independent of AP-1B (Fields et al., 2007). In mock-injected cells as well as in cells coexpressing Arf6D125N, we found LDLR(Y18A) delivered exclusively to the basolateral membrane (99% and 96%, respectively). In contrast, we observed a slight reduction in the fidelity of basolateral delivery when Arf6Q67L was coexpressed (83% basolateral). However, the majority of LDLR(Y18A) was still sorted correctly, which suggests that Arf6 does not play a primary role in LDLR(Y18A) sorting.

As an apical cargo that traverses the REs during biosynthetic delivery, we analyzed the apical variant of VSVGts045-GFP (Ang et al., 2004). A-VSVGts045-GFP is sorted to the apical membrane because of a closer spacing of the GFP moiety to its cytoplasmic tail (i.e., no SP spacer as in the basolaterally sorted VSVGts045-GFP), which seems to obstruct the basolateral sorting signal (Keller et al., 2001). Quantification of total A-VSVG at the surface revealed that 94% of A-VSVG was sorted to the apical membrane in mock-injected cells (Fig. 6 C). In cells coexpressing Arf6D125N, we found that 80% ($P < 0.0001$) of the total A-VSVG was still sorted to the apical membrane (Fig. 6 C). In contrast, in cells coexpressing Arf6Q67L, A-VSVG sorting to the plasma membrane was randomized with only 46% ($P < 0.0001$) of the total signal found at the apical membrane. (Fig. 6 C). Perhaps Arf6Q67L overexpression unmasked the basolateral sorting signal of A-VSVG to some extent perhaps by compromising the sorting fidelity of REs. Regardless, this finding corroborates an important function for Arf6 in REs. Importantly, because Arf6D125N did not lead to basolateral sorting of A-VSVG, we surmise that Arf6 does not normally play a role in A-VSVG sorting.

Finally, we analyzed a cargo, influenza HA, that moves from the TGN into apical early endosomes during apical delivery without passage through REs (Cresawn et al., 2007). Quantification of HA at the surface revealed that 99% of HA was found apically in mock-injected cells. Furthermore, 96% was found apically in cells coexpressing either Arf6D125N or Arf6Q67L.

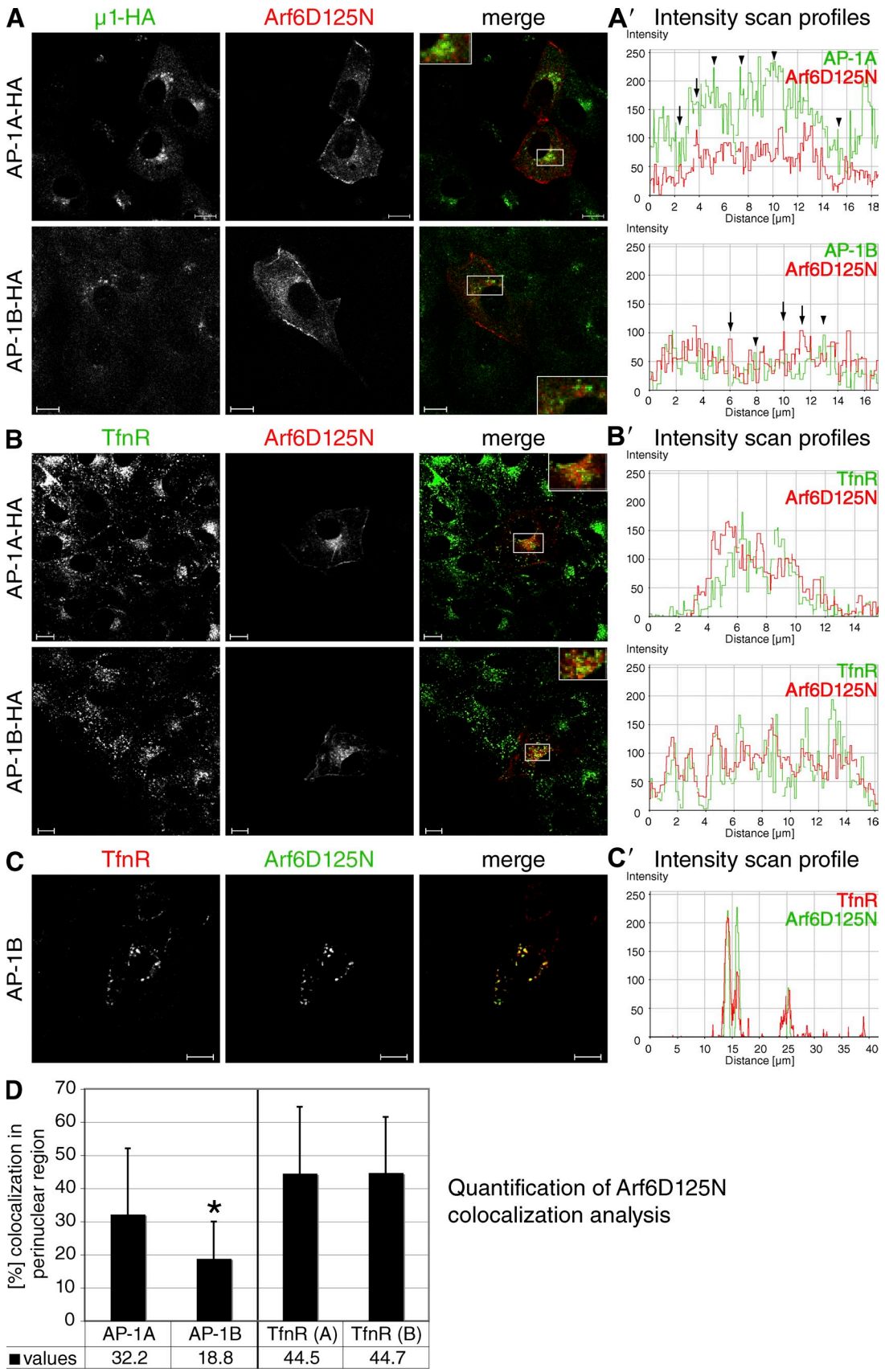

Figure 5. **Arf6D125N partially colocalizes with TfnR but not with AP-1B.** (A and B) LLC-PK1::μ1A-HA or::μ1B-HA cells grown on coverslips for 2 d were transfected with plasmids encoding Arf6D125N-V5. After 21–22 h, cells were fixed and stained for Arf6D125N-V5 and μ1A-HA or μ1B-HA (A), or TfnR (B). Specimens were analyzed by confocal microscopy and representative images are shown. Note that the focal planes in A were adjusted to show maximal perinuclear staining for AP-1A-HA or AP-1B-HA, which may not show maximal perinuclear staining for Arf6D125N. Insets show 2× magnifications of the

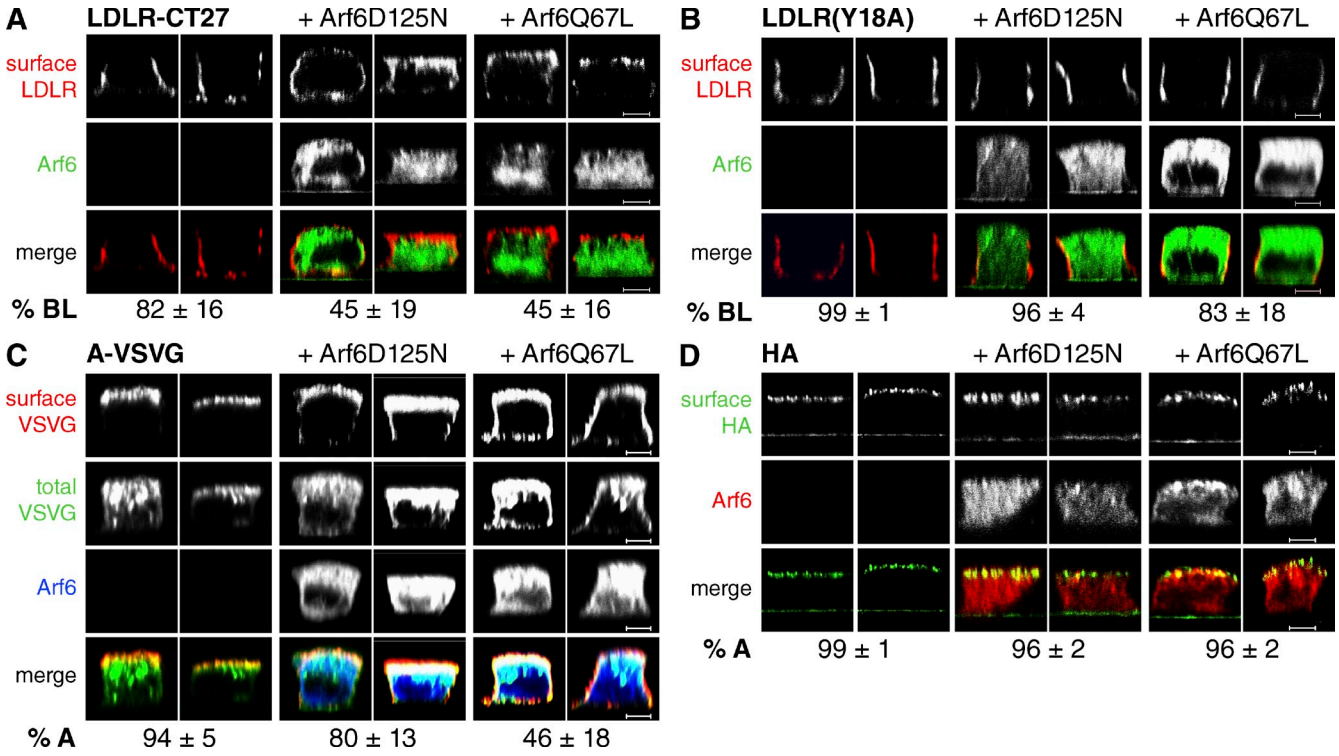

Figure 6. **Arf6 regulates basolateral sorting of AP-1B–dependent cargos.** Polarized, filter-grown MDCK cells were coinjected with plasmids encoding V5-tagged Arf6D125N or V5-tagged Arf6Q67L together with plasmids encoding LDLR-CT27 (A), LDLR(Y18A) (B), A-VSVG (C), or HA (D). (A and B) After microinjection, cells were incubated at 37°C for 1 h followed by 4 h at 20°C and 2 h at 37°C in the presence of CHX. Cells were stained for Arf6-V5 proteins and surface LDLR. For numerical data of LDLR-CT27 sorting, we analyzed 23 mock-injected cells, 24 cells coexpressing Arf6D125N, and 29 cells coexpressing Arf6Q67L from four independent experiments. $P < 0.0001$ for both mutant proteins in comparison to the mock control. To obtain the numerical data for LDLR(Y18A) sorting, we analyzed 29 mock-injected cells, 34 cells coexpressing Arf6D125N, and 27 cells coexpressing Arf6Q67L from at least four independent experiments. $P = 0.0002$ for the pair mock control versus Arf6D125N, and $P < 0.0001$ for the pair mock control versus Arf6Q67L. (C) Cells were incubated and stained as described for VSVG (Fig. 2). Numerical data were gathered by analyzing 26 mock-injected cells, 37 cells coexpressing Arf6D125N, and 37 cells coexpressing Arf6Q67L from three independent experiments. $P < 0.0001$ for both mutant proteins in comparison to the mock control. (D) To express HA after microinjection, cells were incubated for 1 h at 37°C, followed by 4 h at 20°C and 2 h at 37°C in the presence of CHX. Cells were stained for Arf6-V5 proteins and surface HA. We analyzed 28 mock-injected cells, 23 cells coexpressing Arf6D125N, and 26 cells coexpressing Arf6Q67L from four independent experiments to obtain numerical data. Note, because of the green autofluorescence of the filter supports, we quantified lateral and apical pixels for surface HA as opposed to basolateral and apical pixels, as was done in all other cases. $P < 0.0001$ for both mutant proteins versus mock control. (A–D) Specimens were analyzed by confocal microscopy, and representative xz sections are shown. Numerical data were obtained by determining pixel intensities of surface-stained receptors using Volocity software as described in Materials and methods. Data represent mean values, errors are SD. Bars, 5 µm.

In summary, Arf6D125N and Arf6Q67L both inhibited basolateral sorting of AP-1B–dependent cargos VSVG and LDLR-CT27. In addition, Arf6Q67L, but not Arf6D125N, randomized apical delivery of A-VSVG. Importantly, neither Arf6D125N nor Arf6Q67L had any effect on apical delivery of HA.

Knockdown of Arf6 leads to apical missorting of LDLR-CT27

To confirm a role for Arf6 in basolateral sorting, we stably depleted Arf6 in LLC-PK1 cell lines. To this end, we used lentiviruses encoding GFP-tagged short hairpin RNAs (shRNAs) targeting a conserved region of Arf6 transcripts. Lentiviruses targeting glyceraldehyde 3-phosphate dehydrogenase (GAPDH) served as negative controls. Quantitative Western blot analysis revealed that Arf6 levels were reduced by ~90% in cells stably depleted of Arf6 (Fig. 7 A).

We then infected polarized LLC-PK1::µ1B cells stably depleted of Arf6 or GAPDH with defective adenoviruses encoding either LDLR-CT27 or LDLR(Y18A). 24 h after infection, cells were fixed and receptors at the surface were stained. Although ~80% of LDLR-CT27 was localized at the basolateral membrane at steady-state in control cells depleted of GAPDH,

boxed regions. A′ and B′ show representative fluorescence intensity profiles through a region in the boxed area for Arf6D125N and AP-1A, AP-1B, or TfnR. Noncoincidental peaks are marked by arrows (Arf6D125N) or arrowheads (AP-1A-HA or AP-1B-HA). (C) LLC-PK1 cells stably expressing µ1B were seeded onto filter supports. After 3 d, cells were transfected with plasmids encoding Arf6D125N-V5. 21–22 h after transfection, cells were fixed and stained for Arf6D125N-V5 and endogenous TfnR. Shown is a representative focal plane through TfnR-positive REs. Note that the perinuclear concentration of TfnR staining is found in different focal planes dependent on the height of individual cells. Therefore, not all cells in this focal plane show TfnR staining. C′ shows a fluorescence intensity profile through representative REs of the shown focal plane. Bars, 10 µm. (D) The percent overlap between Arf6D125N and AP-1A-HA ($n = 18$), AP-1B-HA ($n = 18$), TfnR in LLC-PK1::µ1A-HA (TfnR[A], $n = 29$), or LLC-PK1::µ1B-HA cells (TfnR[B], $n = 27$) was determined from at least three independent experiments using Volocity software as described in Materials and methods. Error bars indicate SD. *, $P < 0.02$.

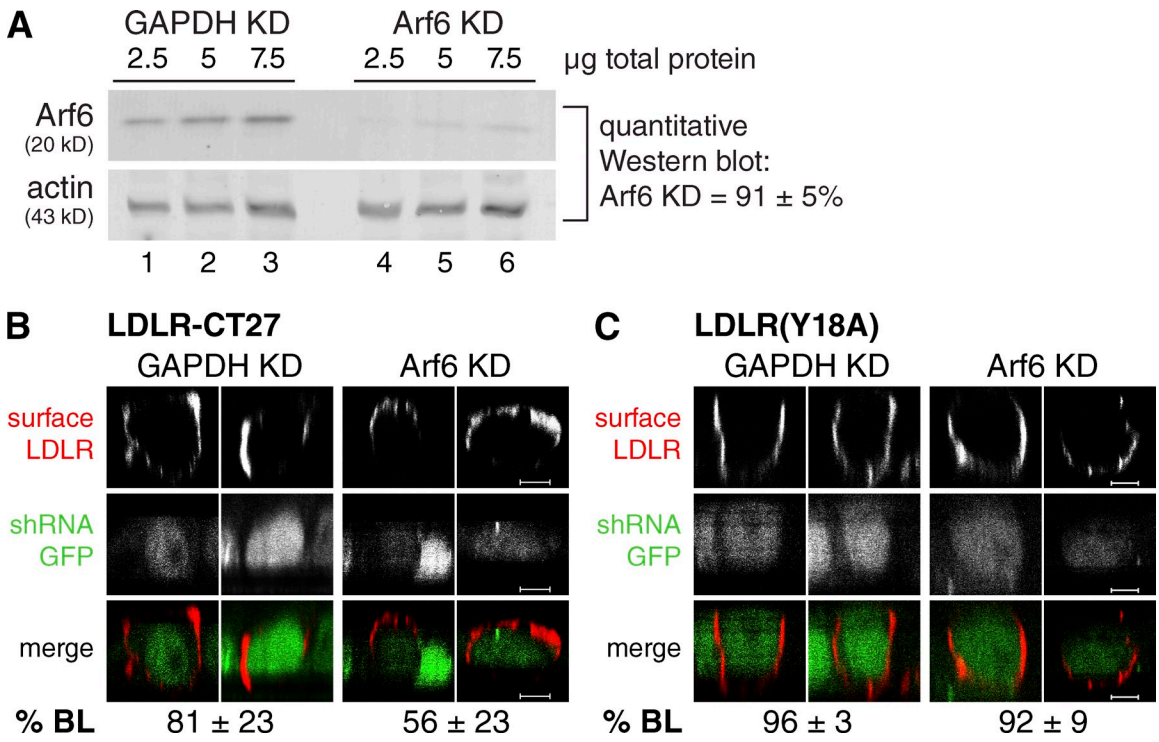

Figure 7. **Arf6 knockdown leads to apical missorting of LDLR-CT27.** (A) Lysates of LLC-PK1::µ1B-HA cells stably depleted of Arf6 or GAPDH were analyzed by SDS-PAGE and quantitative Western blotting as described in Materials and methods. Errors indicate SD. (B and C) LLC-PK1::µ1B cells stably depleted of Arf6 or GAPDH were grown on filter supports and infected with defective adenoviruses encoding LDLR-CT27 (B) or LDLR(Y18A) (C). 24 h after infection, receptors at the surface were stained with anti-LDLR antibodies. GFP fluorescence indicates expression of shRNA. Specimens were analyzed by confocal microscopy, and representative xz sections are shown. We analyzed 28 Arf6 and 32 GAPDH knockdown cells for LDLR-CT27 localization, and 29 Arf6 and 33 GAPDH knockdown cells for LDLR(Y18A) sorting. Numerical data were obtained by determining pixel intensities of receptors stained at the surface using Volocity software as described in Materials and methods. Data represent mean values, errors are SD. $P < 0.0001$ for LDLR-CT27 sorting; $P < 0.02$ for LDLR(Y18A) sorting. Bars, 5 µm.

we found only ∼55% of this receptor at the basolateral membrane in cells depleted of Arf6 ($P < 0.0001$, Fig. 7 B). In contrast, LDLR(Y18A) was found at the basolateral membrane independent of Arf6 expression (Fig. 7 C). Thus, depletion of Arf6 specifically led to apical missorting of an AP-1B–dependent cargo. We conclude that Arf6 plays a major role in basolateral sorting along the AP-1B pathway.

To learn more about the molecular mechanisms that led to apical missorting when Arf6 function was impaired, we investigated AP-1B membrane recruitment either by immunofluorescence or through isolation of clathrin-coated vesicles from LLC-PK1::µ1B-HA cells stably depleted of Arf6 or GAPDH. We did not observe clear effects (unpublished data), perhaps because other Arf proteins might step in for Arf6 (Volpicelli-Daley et al., 2005), without restoring full functionality as judged by LDLR-CT27 missorting. We then investigated Exo70 recruitment. Previously, we showed that AP-1B expression triggered Exo70 and Sec8 recruitment onto REs (Fölsch et al., 2003). Moreover, Arf6 had been shown to interact with Sec10 (Prigent et al., 2003). We did not observe clear changes in Exo70 recruitment in LLC-PK1::µ1B cells stably depleted of Arf6 (unpublished data).

Arf6 recruits AP-1B to plasma membrane protrusions

Finally, we sought an experimental setting that would unambiguously show how Arf6 influences AP-1B localization. Arf6 had been shown to induce lamellipodia when activated in MDCK cells at the edges of cell clusters (Santy and Casanova, 2001; Donaldson, 2003). Because these protrusions contain activated Arf6 (Santy and Casanova, 2001), we wondered whether lamellipodia formation would alter AP-1B distribution. Therefore, we transfected LLC-PK1::µ1B-HA cells grown in small clusters on coverslips with plasmids encoding V5-tagged wild-type Arf6. Transfection of LLC-PK1::µ1A-HA cells was used as a negative control. As shown in Fig. 8, LLC-PK1::µ1B-HA as well as LLC-PK1::µ1A-HA cells growing at the edge of clusters readily formed lamellipodia in response to Arf6 overexpression. Furthermore, in LLC-PK1::µ1B-HA cells, we observed a strong colocalization between Arf6 and AP-1B in cell protrusions in virtually every cell analyzed (Fig. 8, A and A′). In contrast, only little, if any, AP-1A was recruited to Arf6-induced membrane protrusions (Fig. 8, B and B′). Regardless of whether or not AP-1B has a physiological function in membrane ruffles, these data imply that indeed Arf6 specifically recruits AP-1B onto membranes.

Discussion

To gain a mechanistic understanding of AP-1B–mediated sorting, it is essential to unravel how AP-1B is recruited onto REs to initiate cargo selection and formation of clathrin-coated vesicles. With Arf6, we have identified a key regulator of

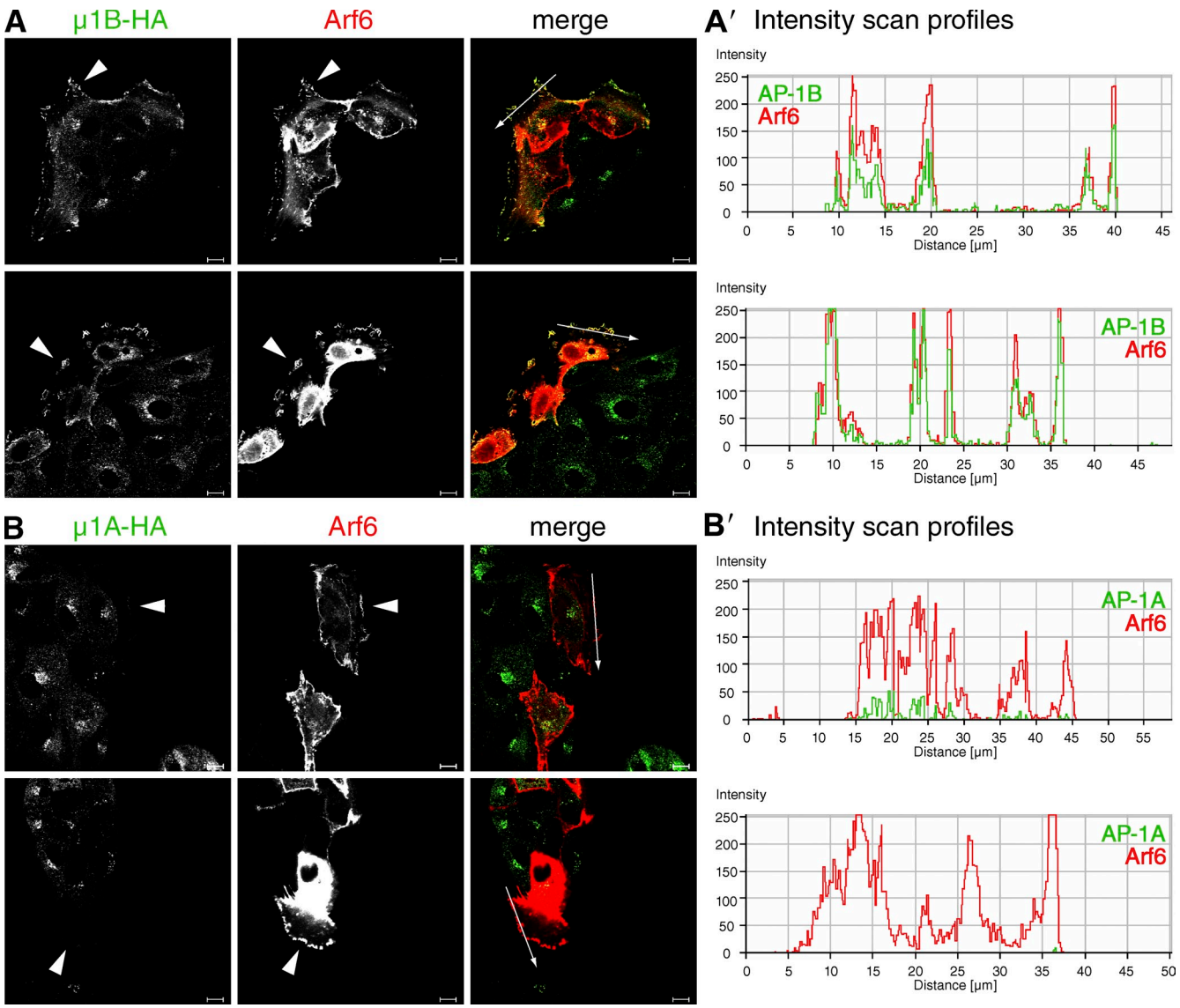

Figure 8. **Arf6 specifically recruits AP-1B into membrane protrusions.** LLC-PK1::μ1B-HA (A) or LLC-PK1::μ1A-HA (B) cells were grown on coverslips. 2 d after seeding, cells were transfected with cDNA encoding V5-tagged Arf6. 21–22 h after transfection, cells were fixed and stained for Arf6-V5 and μ1B-HA or μ1A-HA. Specimens were analyzed by confocal microscopy, and representative images are shown. Arrowheads point to the position of lamellipodia. A′ and B′ show fluorescence intensity profiles of regions in A and B that are indicated by arrows in the merged images. Bars, 10 μm.

AP-1B: Arf6 pulled down AP-1B in vitro and colocalized with AP-1B in TfnR-positive REs. In addition, Arf6 function was needed for proper basolateral targeting of AP-1B–dependent cargos. Furthermore, unlike other regulators that influence intracellular localization of AP-1B (Ang et al., 2003; Fields et al., 2007), Arf6 is the only one found so far that is capable of redirecting AP-1B to a complete different location, i.e., to membrane ruffles forming at plasma membranes. Thus it seems reasonable to assume that Arf6 has a constitutive function in recruiting AP-1B onto REs. In agreement with such a key role of Arf6 are recent findings demonstrating that Arf6 is highly expressed in polarized epithelial cells of mouse tissues (Akiyama et al., 2010).

We found that Arf6 depletion led to apical missorting of LDLR-CT27; however, we did not detect clear effects on AP-1B localization when Arf6 expression was reduced. Perhaps depletion of Arf6 creates a void that may be filled by other Arfs without restoring correct interplay and timing of protein–protein interactions. Indeed, it has been noted previously that Arf functions are somewhat redundant and that Arf proteins had to be depleted in pairs to inhibit membrane trafficking through the Golgi apparatus (Volpicelli-Daley et al., 2005). Alternatively, it might be possible that two Arf proteins work in tandem to ensure proper AP-1B function, as GEFs of the ARNO/cytohesin/Grp1 family had been shown to bind to two Arfs simultaneously, thus functioning as an effector of one and activator of another Arf (Cohen et al., 2007; DiNitto et al., 2007). Regardless, our data indicate a specific need for Arf6.

We identified two Arf6 mutant proteins that are dominant negative for AP-1B function: Arf6D125N and Arf6Q67L. Previously, Arf6 had been known to play a role in endocytosis from the apical membrane in polarized epithelial cells (Altschuler

et al., 1999; Hyman et al., 2006; Wolff et al., 2008). However, initial basolateral targeting of newly synthesized proteins is upstream of postendocytic recycling. Thus, a block in endocytosis would not explain the sorting defects we observed. Furthermore, Arf6 had been found to regulate tight junction integrity mainly via its GEF EFA6 (Luton et al., 2004; Klein et al., 2008). However, under conditions where VSVG and LDLR-CT27 were delivered to the apical membrane, the tight junctions remained intact (Fig. S1), ruling out the possibility that disrupted tight junctions led to missorting in our assay. Still, the dominant-negative Arf6 mutant protein, Arf6T27N, had been shown to localize to adherens junction (Palacios et al., 2001), which might explain why we did not observe missorting of VSVG in the presence of Arf6T27N. It simply might not be very effective in sequestering Arf6 GEFs in REs.

It is further unlikely that Arf6Q67L inhibits basolateral sorting by just sequestering AP-1B. If that were the case, we would have expected a similar inhibition of basolateral sorting upon overexpression of Arf1Q71L because both active mutant proteins pull down comparable amounts of AP-1B in vitro (Fig. 1). Perhaps in vivo, productive interaction between adaptor complexes and Arf GTPases requires membrane localization. Indeed, the cytosolic form of Arf6Q67L—Arf6Q67L/G2A—was a less potent inhibitor of VSVG sorting than membrane-bound Arf6Q67L (Fig. 4). Unfortunately, transient expression of Arf6Q67L in LLC-PK1 cells was toxic; therefore, we could not analyze whether AP-1B and Arf6Q67L may colocalize. Regardless, in the future it will be interesting to learn how hetero-tetrameric adaptor complexes such as AP-1B interact with active, membrane-localized Arf proteins.

Interestingly, Arf6D125N failed to colocalize with AP-1B, though it still colocalized with TfnR in REs. These data indicate that perhaps active Arf6 is needed for linking AP-1B recruitment onto REs with productive cargo selection. Arf6D125N may inhibit the activation of endogenous Arf6 by sequestering its GEFs in REs. Intriguingly, AP-1B is not totally displaced from its perinuclear localization in the presence of Arf6D125N. Previously, we showed that $PI(3,4,5)P_3$ was necessary for AP-1B recruitment onto REs (Fields et al., 2010). Perhaps $PI(3,4,5)P_3$ is responsible for residual AP-1B localization in REs when Arf6D125N is expressed, without being able to sustain basolateral sorting of AP-1B cargos. Indeed, our data indicate that overexpression of Arf6D125N (or Arf6Q67L) has only moderate effects on $PI(3,4,5)P_3$ levels in REs. These data also indirectly argue that Arf6 may not regulate AP-1B function via activation of PIPKIγ-90 and influencing $PI(3,4,5)P_3$ levels. In fact, not only Arf6 but also AP-1B itself is able to bind and activate PIPKIγ-90 (Krauss et al., 2006; Ling et al., 2007), and AP-1B expression is necessary for PIPKIγ-90 localization in REs (Fields et al., 2010). This indicates that perhaps spatial and temporal activation of PIPKIγ-90 may be regulated by both Arf6 and AP-1B.

Previously, Arf6 was mainly found localizing at the plasma membrane (Cavenagh et al., 1996), which is in agreement with its functions in endocytosis (D'Souza-Schorey and Chavrier, 2006). However, there were also findings of endosomal Arf6 localization (Marshansky et al., 1997; Song et al., 1998). Here we show that in AP-1B–positive epithelial cells, Arf6 localizes to TfnR-positive REs. This dual localization and function of proteins at the plasma membrane and in REs has already been described for other factors such as PIPKIγ-90 (Ling et al., 2007; Fields et al., 2010) and ARH (Kang and Fölsch, 2011). This implies similarities between REs and the plasma membrane with regard to biochemical identity. Indeed, $PI(3,4,5)P_3$ accumulates at the leading edge of migrating cells (Franca-Koh et al., 2007), the basolateral plasma membrane (Gassama-Diagne et al., 2006), and in REs (Fields et al., 2010). Thus, it may not be entirely surprising that we found AP-1B localizing to the plasma membrane in response to Arf6 activation, and it will be interesting to learn whether AP-1B has a function at the plasma membrane under these conditions.

In conclusion, data presented in this study strongly imply a regulatory function for Arf6 in AP-1B–mediated protein sorting, most likely through recruitment of AP-1B onto $PI(3,4,5)P_3$-positive REs.

Materials and methods

Cloning procedures and shRNA constructs

HA-tagged versions of wild-type Arf6, Arf6T27N, and Arf6Q67L were received from P. Chavrier (Institut Curie, Paris, France). These cDNAs were subsequently used as PCR templates using Arf6-a and Arf6-b as primers, thereby introducing a C-terminal V5-tag (Table S1). PCR products were cloned as KpnI–XbaI fragments into pShuttle-CMV. V5-tagged Arf6 wild type and mutants were then amplified using primers Arf6-c and Arf6-d (Table S1) to generate PCR products with EcoRI and HindIII restriction sites for cloning into the microinjection vector pRKV. To generate GST fusion proteins, V5-tagged Arf6 wild type and mutants were amplified using primers Arf6-e and Arf6-f (Table S1), which introduced BglII and XhoI restriction sites for cloning of V5-tagged Arf6 in frame behind GST into pGEX-6P-1.

For site-directed mutagenesis of Arf6, we performed QuikChange mutagenesis (Agilent Technologies) using V5-tagged Arf6 in pShuttle as a template with corresponding sense and anti-sense primers. The sense primer for the generation of Arf6D125N was Arf6-D125N (Table S1), and the sense primer for Arf6N48I generation was Arf6-N48I (Table S1). To generate Arf6Q67L/Q37E/S38I, we used V5-tagged Arf6Q67L as template, and the sense primer was Arf6-QS (Table S1). To generate G2A mutations, we used V5-tagged Arf6Q67L or V5-tagged Arf6D125N in pShuttle as templates, and the Arf6-G2A as N-terminal and Arf6-d as C-terminal primer for cloning of Arf6Q67L/G2A or Arf6D125N/G2A into pRKV.

To clone GST fusions of Arf1 in which the N-terminal 17 amino acids had been deleted (Δ17Arf1), we used His-tagged fusion constructs of wild-type Arf1 or Arf1Q71L provided to us by G. Warren (Max F. Perutz Laboratories, Vienna, Austria) and J. Donaldson (National Institutes of Health, Bethesda, MD) as templates and Arf1-a and Arf1-b primers (Table S1) to generate PCR products with BamHI and XhoI restriction sites for cloning into pGEX-6P-1. Arf1T31N was generated by site-directed mutagenesis using Arf1-T31N as the sense primer and wild-type Arf1 as a template. V5-tagged Arf1T31N and V5-tagged Arf1Q71L were first cloned into pShuttle-CMV as PCR fragments using Arf1-c and Arf1-d (Table S1) as primers, thereby introducing C-terminal V5 tags. Arf1T31N-V5 and Arf1Q71L-V5 were subsequently subcloned as BglII–XbaI fragments from pShuttle into pRKV.

Plasmids encoding VSVGts045-GFP, A-VSVG-GFP, LDLR-CT27, LDLR(Y18A), or HA have been described previously (Nokes et al., 2008). Plasmids encoding PH-Akt-GFP were a gift from P. Devreotes (Johns Hopkins School of Medicine, Baltimore, MD). Defective adenoviruses encoding LDLR-CT27 or LDLR(Y18A) have been described previously (Fields et al., 2007).

The shRNAmir construct in the lentiviral vector pGIPz targeting human, mouse, and rat (and porcine) Arf6 (oligo ID V2LMM_67737, sequence was: 5′-TGCTGTTGACAGTGAGCGAGCTCACATGGTTAACCTCTAATAGTGAAGCCACAGATGTATTAGAGGTTAACCATGTGAGCCTGCCTACTGCCTCGGA-3′) was obtained from Thermo Fisher Scientific. The construct targeting human GAPDH was as described previously

(Nokes et al., 2008). Replication-defective lentiviruses were produced by cotransfecting pGIPz, pMD2G, and psPAX2 into HEK293T cells using a standard method (Salmon and Trono, 2006).

Antibodies

Mouse monoclonal antibodies were as follows: anti-HA (16B12) from BabCo, anti–γ-adaptin (88) and anti-GM130 (610822) from BD, anti-acetylated tubulin (6-11B-1) from Sigma-Aldrich, anti-ZO-1 from Invitrogen, and anti-actin (C4) from Millipore. Anti-V5 antibodies were generated by R. Randall (University of St. Andrews, St. Andrews, Fife, Scotland, UK) and obtained from R. Lamb (Northwestern University, Evanston, IL). Rabbit polyclonal antibodies recognizing GFP (ab90) were from Abcam, antibodies recognizing GST (A-5800) were from Invitrogen, and anti-Arf6 antibodies were a gift from J. Donaldson (NIH, Bethesda, MD). Goat polyclonal antibodies directed against the ectodomain of HA (anti-H3 [A/HongKong/1/68], NR-3118) were obtained through the National Institutes of Health Biodefense and Emerging Infections Research Resources Repository (National Institute of Allergy and Infectious Diseases). Hybridoma cell lines producing antibodies directed against LDLR (C7), TfnR (H68.4), gp58, or VSVG (TK1) have been described previously (Fields et al., 2007).

Secondary antibodies labeled with Alexa Fluor fluorophores were purchased from Invitrogen, Cy5-labeled secondary antibodies were from Jackson ImmunoResearch Laboratories or SouthernBiotech, and HRP-conjugated antibodies were from Jackson ImmunoResearch Laboratories.

Cell culture and immunofluorescence analysis

All cells were grown at 37°C in the presence of 5% CO_2, and media were supplemented with 0.1 mg/ml penicillin/streptomycin and 2 mM L-glutamine unless stated otherwise. MDCK cells were maintained in MEM (7% fetal bovine serum). 3T3 fibroblasts were grown in DME (10% fetal bovine serum, 4 mM L-glutamine), and EFA47 cells were maintained in DME (10% fetal bovine serum) and 200 µg/ml hygromycin. HEK293T cells were grown in DME (10% fetal bovine serum) on plates coated with fibronectin and collagen (Nokes et al., 2008). LLC-PK1::µ1A-HA, LLC-PK1::µ1B-HA, and LLC-PK1::µ1B cells were grown in α-MEM (7% fetal bovine serum) containing 1 mg/ml geneticin. Finally, HEK293 cells for amplification of defective adenoviruses were grown in DME (10% fetal bovine serum).

LLC-PK1::µ1B cells depleted of Arf6 or GAPDH were generated by infecting the cells with lentiviruses encoding shRNAs targeting Arf6 or GAPDH, respectively. 24–48 h after infection, growth media were supplemented with 16 µg/ml puromycin to select and subsequently maintain infected cells (Anderson et al., 2005). Cells were used for experiments as soon as possible after selection with puromycin.

For experiments with polarized cells, MDCK or LLC-PK1::µ1B cells were seeded at a density of 4×10^5 cells per 12-mm filter (0.4 µg pore size; Corning) and cultured for 3–4 d with changes of medium in the basolateral chambers every day. For microinjection experiments, cells were seeded onto clear filters. For immunofluorescence experiments with cells grown on coverslips, cells were seeded onto Alcian Blue–coated coverslips and grown for 3–4 d. Transient transfections were performed using Lipofectamine 2000 (Invitrogen) according to the manufacturer's instructions.

Infections of filter-grown LLC-PK1 cells depleted of Arf6 or GAPDH with defective adenoviruses were performed 3 d after seeding in serum-free media with the viruses added to the apical chamber and gentle rocking at 37°C for 2 h. Media were then exchanged with regular growth media. After ∼24 h, cells were processed for immunofluorescence microscopy as described below.

Microinjection of cells was performed exactly as described previously (Nokes et al., 2008), using a Femtojet microinjector (Injectman NI2; Eppendorf) mounted on an inverted microscope (Axiovert 200, Carl Zeiss) with a heated stage. In brief, cells grown on filter supports were placed in Hepes-buffered media (50 mM Hepes) and microinjected with 0.2 mg/ml cDNAs at 39°C (VSVG) or 37°C (LDLR mutant proteins and HA). After injection, cells were typically further incubated at the microinjection temperature or 20°C, followed by a chase at 31°C (VSVG) or 37°C (non-VSVG cargos) for 1–2 h in the presence of 0.1 mg/ml CHX (see figure legends for details on incubation times).

Cell surface staining, fixation of the cells in 3% paraformaldehyde for 15 min at room temperature, and staining of fixed cells was performed essentially as described previously (Nokes et al., 2008). In brief, for surface staining, cells were directly incubated with primary antibodies directed against the ectodomain of transmembrane receptors on ice for 1 h before fixation and permeabilization of the cells. To permeabilize cells after fixation, probes were incubated for 1 h in a blocking/permeabilization buffer (BPB; 2% [wt/vol] BSA, 0.4% [wt/vol] saponin in PBS^{2+} [PBS {0.2 g/liter KCl, 0.2 g/liter KH_2PO_4, 8 g/liter NaCl, and 2.17 g/liter $Na_2HPO_4 \times 7\ H_2O$} plus 0.1 g/liter $CaCl_2$ and 0.1 g/liter $MgCl_2 \times 6\ H_2O$]) with 10% [vol/vol] goat serum. After permeabilization, cells were incubated with primary antibodies diluted in BPB for 1 h, washed, and subsequently incubated with secondary antibodies diluted in BPB for 1 h. Cells were mounted in a water solution containing 10% [wt/vol] DABCO and 50% [wt/vol] glycerol.

Specimens were analyzed at room temperature using a confocal microscope (Microsystem LSM 510 with ConfoCor3 software; Carl Zeiss) equipped with a C-Apochromat 63× 1.2 NA water immersion objective lens or a confocal microscope (LSM 510; Zen software) equipped with a Plan-Apochromat 63× 1.4 oil immersion objective lens for Fig. 8 (all from Carl Zeiss). Images were adjusted using Photoshop (Adobe) and combined using Illustrator (Adobe).

GST pull-down assays

GST fusion proteins were produced in and purified out of *E. coli* using GSTrap columns from GE Healthcare according to the manufacturer's recommendations and desalted subsequently. The concentrations of purified proteins were determined using the BCA assay from Thermo Fisher Scientific and adjusted with respect to Western blot signals in comparison to GST.

For pull-downs, 0.5 mg GST or GST fusion protein were bound to glutathione Sepharose beads (GE Healthcare) in the presence of 2 mM $MgCl_2$ and 1 mM nucleotide (GDP for Arf1T31N, Arf6T27N, and Arf6D125N; GTP for Arf1Q71L, Arf6Q67L, and Arf6Q67L/Q37E/S38I) in PBS buffer (2.7 mM KCl, 1.5 mM KH_2PO_4, 137 mM NaCl, and 8.1 mM Na_2HPO_4) for 1 h at 4°C by end-over-end rotation. Beads were then washed three times with cell lysis buffer (20 mM Hepes, pH 7.4, 320 mM Sucrose, 2 mM $MgCl_2$, 1% Triton X-100 [w/vol], 1 mM appropriate nucleotide, and 1× protease inhibitors [Boehringer] in PBS). Subsequently, the beads were incubated with 1 ml of cell lysate in lysis buffer (∼3 µg total protein) by end-over-end rotation at 4°C for 4 h. Beads were extensively washed and extracted with SDS sample buffer. Samples were analyzed by SDS-PAGE and Western blotting. Western blots were developed using SuperSignal West Pico chemiluminescent substrate (Thermo Fisher Scientific). Developed films were scanned using a Perfection 4490 photoscanner (Epson). Data were directly imported into Photoshop software and combined using Illustrator. Data for each pull-down experiment were obtained from one gel with the same exposure time and exactly the same alterations in Photoshop.

Quantitative Western blots

For quantitative Western blot analysis, we used an FLA-5100 Fluor Imager (Image Reader FLA-5000 series V1.0 software; FujiFilm) to scan blots that were decorated with anti-Arf6 or anti-actin primary antibodies and Alexa Fluor 488–labeled secondary antibodies. Scanned blots were then analyzed using MultiGauge software (FujiFilm). Arf6 expression in cells depleted of GAPDH was set as 100%. We analyzed three independent experiments carrying three different data points each (2.5, 5, and 7.5 µg total protein). For graphic display, scanned images were imported into Photoshop, and cropped images were assembled in Illustrator.

To generate cell lysates, LLC-PK1 cells stably knocking down Arf6 or GAPDH were seeded at a 1:1 dilution onto 10-cm plates. After 24 h, cells were harvested and cracked using a ball-bearing homogenizer in 1 ml Hepes buffer (150 mM NaCl, 10 mM Hepes, pH 7.3, 0.5 mM $MgCl_2$, 0.02% [w/vol] NaN_3, and 1× protease inhibitors [Boehringer Ingelheim GmbH]), followed by a clarifying spin at 13,000 rpm for 20 min at 4°C (Eppendorf microcentrifuge). Protein concentrations were determined using the BCA assay (Thermo Fisher Scientific), and 2.5, 5, and 7.5 µg of total protein were run on SDS gels, and blotted onto Immobilon FL membranes (Millipore).

Statistical analysis of immunofluorescence data

To determine the percentage of basolateral or apical localization of receptors at the surface, TIFF files of confocal xz sections were imported into Volocity 4.4 software (PerkinElmer). We then determined the total amount of pixels at the basolateral (lateral membrane only for HA because of the autofluorescence of the filters) or apical membranes by circling the respective membrane areas as areas of interest. We then calculated the percent values of basolateral or apical receptor based on these data.

Colocalization was determined by importing confocal raw data into Volocity 4.4 software (PerkinElmer). Note that we only analyzed cells with low-to-moderate expression levels of exogenously expressed markers to avoid saturation. For all images analyzed, we set the threshold levels to the

exact same value. We then circled the region of perinuclear TfnR, AP-1B–HA, or AP-1A–HA staining as the region of interest for the calculation of the Manders overlap coefficients, which were directly converted to percent overlap values (i.e., a Manders coefficient of 0.5 indicates that 50% of the pixels overlap; Manders et al., 1993). To determine percent localization at the plasma membrane, we calculated the total pixels and interior pixels only of a cell. The amount of signal at the plasma membrane was then calculated using these numbers.

To determine statistical significance, we first calculated the mean value and SD for each experimental condition. Mean values, SD, and *n* values were then used to calculate P-values in an unpaired student's *t* test using QuickCals (GraphPad Software).

Online supplemental material

Fig. S1 demonstrates that overexpression of Arf6Q67L or Arf6D125 in MDCK cells using a microinjection technique does not interfere with overall polarity. Fig. S2 depicts the effects of Arf6D125N or Arf6Q67L overexpression on the localization of PH-Akt-GFP using transient transfection in MDCK cells. Table S1 shows the sequences of primers used in PCR reactions. Online supplemental material is available at http://www.jcb.org/cgi/content/full/jcb.201106010/DC1.

We would like to thank Drs. Philippe Chavrier, Peter Devreotes, Julie Donaldson, Robert Lamb, and Graham Warren for the generous gifts of reagents, and Julie Jackson and Ian C. Fields for expert technical assistance. We are grateful to Dr. Bettina Winckler (University of Virginia, Charlottesville, VA) for comments on the manuscript.

This work was funded by grants from the National Institutes of Health (GM070736 and GM070736-05S1) to H. Fölsch.

Submitted: 1 June 2011
Accepted: 12 August 2011

References

Akiyama, M., M. Zhou, R. Sugimoto, T. Hongu, M. Furuya, Y. Funakoshi, M. Kato, H. Hasegawa, and Y. Kanaho. 2010. Tissue- and development-dependent expression of the small GTPase Arf6 in mice. *Dev. Dyn.* 239:3416–3435. http://dx.doi.org/10.1002/dvdy.22481

Al-Awar, O., H. Radhakrishna, N.N. Powell, and J.G. Donaldson. 2000. Separation of membrane trafficking and actin remodeling functions of ARF6 with an effector domain mutant. *Mol. Cell. Biol.* 20:5998–6007. http://dx.doi.org/10.1128/MCB.20.16.5998-6007.2000

Altschuler, Y., S. Liu, L. Katz, K. Tang, S. Hardy, F. Brodsky, G. Apodaca, and K. Mostov. 1999. ADP-ribosylation factor 6 and endocytosis at the apical surface of Madin-Darby canine kidney cells. *J. Cell Biol.* 147:7–12. http://dx.doi.org/10.1083/jcb.147.1.7

Anderson, E., S. Maday, J. Sfakianos, M. Hull, B. Winckler, D. Sheff, H. Fölsch, and I. Mellman. 2005. Transcytosis of NgCAM in epithelial cells reflects differential signal recognition on the endocytic and secretory pathways. *J. Cell Biol.* 170:595–605. http://dx.doi.org/10.1083/jcb.200506051

Ang, A.L., H. Fölsch, U.M. Koivisto, M. Pypaert, and I. Mellman. 2003. The Rab8 GTPase selectively regulates AP-1B-dependent basolateral transport in polarized Madin-Darby canine kidney cells. *J. Cell Biol.* 163:339–350. http://dx.doi.org/10.1083/jcb.200307046

Ang, A.L., T. Taguchi, S. Francis, H. Fölsch, L.J. Murrells, M. Pypaert, G. Warren, and I. Mellman. 2004. Recycling endosomes can serve as intermediates during transport from the Golgi to the plasma membrane of MDCK cells. *J. Cell Biol.* 167:531–543. http://dx.doi.org/10.1083/jcb.200408165

Austin, C., M. Boehm, and S.A. Tooze. 2002. Site-specific cross-linking reveals a differential direct interaction of class 1, 2, and 3 ADP-ribosylation factors with adaptor protein complexes 1 and 3. *Biochemistry*. 41:4669–4677. http://dx.doi.org/10.1021/bi016064j

Boehm, M., and J.S. Bonifacino. 2001. Adaptins: the final recount. *Mol. Biol. Cell*. 12:2907–2920.

Brodsky, F.M., C.Y. Chen, C. Knuehl, M.C. Towler, and D.E. Wakeham. 2001. Biological basket weaving: formation and function of clathrin-coated vesicles. *Annu. Rev. Cell Dev. Biol.* 17:517–568. http://dx.doi.org/10.1146/annurev.cellbio.17.1.517

Cavenagh, M.M., J.A. Whitney, K. Carroll, C. Zhang, A.L. Boman, A.G. Rosenwald, I. Mellman, and R.A. Kahn. 1996. Intracellular distribution of Arf proteins in mammalian cells. Arf6 is uniquely localized to the plasma membrane. *J. Biol. Chem.* 271:21767–21774. http://dx.doi.org/10.1074/jbc.271.36.21767

Citterio, C., A. Vichi, G. Pacheco-Rodriguez, A.M. Aponte, J. Moss, and M. Vaughan. 2008. Unfolded protein response and cell death after depletion of brefeldin A-inhibited guanine nucleotide-exchange protein GBF1. *Proc. Natl. Acad. Sci. USA*. 105:2877–2882. http://dx.doi.org/10.1073/pnas.0712224105

Cohen, L.A., A. Honda, P. Varnai, F.D. Brown, T. Balla, and J.G. Donaldson. 2007. Active Arf6 recruits ARNO/cytohesin GEFs to the PM by binding their PH domains. *Mol. Biol. Cell*. 18:2244–2253. http://dx.doi.org/10.1091/mbc.E06-11-0998

Cook, R.N., S.F. Ang, R.S. Kang, and H. Fölsch. 2011. Analyzing the function of small GTPases by microinjection of plasmids into polarized epithelial cells. *J. Vis. Exp.* 51:2645. http://dx.doi.org/10.3791/2645

Cresawn, K.O., B.A. Potter, A. Oztan, C.J. Guerriero, G. Ihrke, J.R. Goldenring, G. Apodaca, and O.A. Weisz. 2007. Differential involvement of endocytic compartments in the biosynthetic traffic of apical proteins. *EMBO J.* 26:3737–3748. http://dx.doi.org/10.1038/sj.emboj.7601813

DiNitto, J.P., A. Delprato, M.T. Gabe Lee, T.C. Cronin, S. Huang, A. Guilherme, M.P. Czech, and D.G. Lambright. 2007. Structural basis and mechanism of autoregulation in 3-phosphoinositide-dependent Grp1 family Arf GTPase exchange factors. *Mol. Cell*. 28:569–583. http://dx.doi.org/10.1016/j.molcel.2007.09.017

Donaldson, J.G. 2003. Multiple roles for Arf6: sorting, structuring, and signaling at the plasma membrane. *J. Biol. Chem.* 278:41573–41576. http://dx.doi.org/10.1074/jbc.R300026200

D'Souza-Schorey, C., and P. Chavrier. 2006. ARF proteins: roles in membrane traffic and beyond. *Nat. Rev. Mol. Cell Biol.* 7:347–358. http://dx.doi.org/10.1038/nrm1910

D'Souza-Schorey, C., E. van Donselaar, V.W. Hsu, C. Yang, P.D. Stahl, and P.J. Peters. 1998. ARF6 targets recycling vesicles to the plasma membrane: insights from an ultrastructural investigation. *J. Cell Biol.* 140:603–616. http://dx.doi.org/10.1083/jcb.140.3.603

Eskelinen, E.L., C. Meyer, H. Ohno, K. von Figura, and P. Schu. 2002. The polarized epithelia-specific mu 1B-adaptin complements mu 1A-deficiency in fibroblasts. *EMBO Rep.* 3:471–477. http://dx.doi.org/10.1093/embo-reports/kvf092

Fields, I.C., E. Shteyn, M. Pypaert, V. Proux-Gillardeaux, R.S. Kang, T. Galli, and H. Fölsch. 2007. v-SNARE cellubrevin is required for basolateral sorting of AP-1B-dependent cargo in polarized epithelial cells. *J. Cell Biol.* 177:477–488. http://dx.doi.org/10.1083/jcb.200610047

Fields, I.C., S.M. King, E. Shteyn, R.S. Kang, and H. Fölsch. 2010. Phosphatidylinositol 3,4,5-trisphosphate localization in recycling endosomes is necessary for AP-1B-dependent sorting in polarized epithelial cells. *Mol. Biol. Cell*. 21:95–105. http://dx.doi.org/10.1091/mbc.E09-01-0036

Fölsch, H. 2005. The building blocks for basolateral vesicles in polarized epithelial cells. *Trends Cell Biol.* 15:222–228. http://dx.doi.org/10.1016/j.tcb.2005.02.006

Fölsch, H., H. Ohno, J.S. Bonifacino, and I. Mellman. 1999. A novel clathrin adaptor complex mediates basolateral targeting in polarized epithelial cells. *Cell*. 99:189–198. http://dx.doi.org/10.1016/S0092-8674(00)81650-5

Fölsch, H., M. Pypaert, P. Schu, and I. Mellman. 2001. Distribution and function of AP-1 clathrin adaptor complexes in polarized epithelial cells. *J. Cell Biol.* 152:595–606. http://dx.doi.org/10.1083/jcb.152.3.595

Fölsch, H., M. Pypaert, S. Maday, L. Pelletier, and I. Mellman. 2003. The AP-1A and AP-1B clathrin adaptor complexes define biochemically and functionally distinct membrane domains. *J. Cell Biol.* 163:351–362. http://dx.doi.org/10.1083/jcb.200309020

Fölsch, H., P.E. Mattila, and O.A. Weisz. 2009. Taking the scenic route: biosynthetic traffic to the plasma membrane in polarized epithelial cells. *Traffic*. 10:972–981. http://dx.doi.org/10.1111/j.1600-0854.2009.00927.x

Franca-Koh, J., Y. Kamimura, and P.N. Devreotes. 2007. Leading-edge research: PtdIns(3,4,5)P3 and directed migration. *Nat. Cell Biol.* 9:15–17. http://dx.doi.org/10.1038/ncb0107-15

Gassama-Diagne, A., W. Yu, M. ter Beest, F. Martin-Belmonte, A. Kierbel, J. Engel, and K. Mostov. 2006. Phosphatidylinositol-3,4,5-trisphosphate regulates the formation of the basolateral plasma membrane in epithelial cells. *Nat. Cell Biol.* 8:963–970. http://dx.doi.org/10.1038/ncb1461

Hirst, J., and M.S. Robinson. 1998. Clathrin and adaptors. *Biochim. Biophys. Acta*. 1404:173–193. http://dx.doi.org/10.1016/S0167-4889(98)00056-1

Hyman, T., M. Shmuel, and Y. Altschuler. 2006. Actin is required for endocytosis at the apical surface of Madin-Darby canine kidney cells where ARF6 and clathrin regulate the actin cytoskeleton. *Mol. Biol. Cell*. 17:427–437. http://dx.doi.org/10.1091/mbc.E05-05-0420

Jovanovic, O.A., F.D. Brown, and J.G. Donaldson. 2006. An effector domain mutant of Arf6 implicates phospholipase D in endosomal membrane recycling. *Mol. Biol. Cell*. 17:327–335. http://dx.doi.org/10.1091/mbc.E05-06-0523

Kang, R.S., and H. Fölsch. 2011. ARH cooperates with AP-1B in the exocytosis of LDLR in polarized epithelial cells. *J. Cell Biol.* 193:51–60. http://dx.doi.org/10.1083/jcb.201012121

Keller, P., D. Toomre, E. Díaz, J. White, and K. Simons. 2001. Multicolour imaging of post-Golgi sorting and trafficking in live cells. *Nat. Cell Biol.* 3:140–149. http://dx.doi.org/10.1038/35055042

Klausner, R.D., J.G. Donaldson, and J. Lippincott-Schwartz. 1992. Brefeldin A: insights into the control of membrane traffic and organelle structure. *J. Cell Biol.* 116:1071–1080. http://dx.doi.org/10.1083/jcb.116.5.1071

Klein, S., M. Partisani, M. Franco, and F. Luton. 2008. EFA6 facilitates the assembly of the tight junction by coordinating an Arf6-dependent and -independent pathway. *J. Biol. Chem.* 283:30129–30138. http://dx.doi.org/10.1074/jbc.M803375200

Knorr, T., W. Nagel, and W. Kolanus. 2000. Phosphoinositides determine specificity of the guanine-nucleotide exchange activity of cytohesin-1 for ADP-ribosylation factors derived from a mammalian expression system. *Eur. J. Biochem.* 267:3784–3791. http://dx.doi.org/10.1046/j.1432-1327.2000.01416.x

Krauss, M., M. Kinuta, M.R. Wenk, P. De Camilli, K. Takei, and V. Haucke. 2003. ARF6 stimulates clathrin/AP-2 recruitment to synaptic membranes by activating phosphatidylinositol phosphate kinase type Iγ. *J. Cell Biol.* 162:113–124. http://dx.doi.org/10.1083/jcb.200301006

Krauss, M., V. Kukhtina, A. Pechstein, and V. Haucke. 2006. Stimulation of phosphatidylinositol kinase type I-mediated phosphatidylinositol (4,5)-bisphosphate synthesis by AP-2mu-cargo complexes. *Proc. Natl. Acad. Sci. USA.* 103:11934–11939. http://dx.doi.org/10.1073/pnas.0510306103

Ling, K., S.F. Bairstow, C. Carbonara, D.A. Turbin, D.G. Huntsman, and R.A. Anderson. 2007. Type Iγ phosphatidylinositol phosphate kinase modulates adherens junction and E-cadherin trafficking via a direct interaction with μ1B adaptin. *J. Cell Biol.* 176:343–353. http://dx.doi.org/10.1083/jcb.200606023

Luton, F., S. Klein, J.P. Chauvin, A. Le Bivic, S. Bourgoin, M. Franco, and P. Chardin. 2004. EFA6, exchange factor for ARF6, regulates the actin cytoskeleton and associated tight junction in response to E-cadherin engagement. *Mol. Biol. Cell.* 15:1134–1145. http://dx.doi.org/10.1091/mbc.E03-10-0751

Macia, E., F. Luton, M. Partisani, J. Cherfils, P. Chardin, and M. Franco. 2004. The GDP-bound form of Arf6 is located at the plasma membrane. *J. Cell Sci.* 117:2389–2398. http://dx.doi.org/10.1242/jcs.01090

Manders, E.M.M., F.J. Verbeek, and J.A. Aten. 1993. Measurement of co-localization of objects in dual-colour confocal images. *J. Microsc.* 169:375–382. http://dx.doi.org/10.1111/j.1365-2818.1993.tb03313.x

Marshansky, V., S. Bourgoin, I. Londoño, M. Bendayan, and P. Vinay. 1997. Identification of ADP-ribosylation factor-6 in brush-border membrane and early endosomes of human kidney proximal tubules. *Electrophoresis*. 18:538–547. http://dx.doi.org/10.1002/elps.1150180334

Martin-Belmonte, F., and K. Mostov. 2008. Regulation of cell polarity during epithelial morphogenesis. *Curr. Opin. Cell Biol.* 20:227–234. http://dx.doi.org/10.1016/j.ceb.2008.01.001

Mellman, I., and W.J. Nelson. 2008. Coordinated protein sorting, targeting and distribution in polarized cells. *Nat. Rev. Mol. Cell Biol.* 9:833–845. http://dx.doi.org/10.1038/nrm2525

Nakatsu, F., and H. Ohno. 2003. Adaptor protein complexes as the key regulators of protein sorting in the post-Golgi network. *Cell Struct. Funct.* 28:419–429. http://dx.doi.org/10.1247/csf.28.419

Nie, Z., and P.A. Randazzo. 2006. Arf GAPs and membrane traffic. *J. Cell Sci.* 119:1203–1211. http://dx.doi.org/10.1242/jcs.02924

Nokes, R.L., I.C. Fields, R.N. Collins, and H. Fölsch. 2008. Rab13 regulates membrane trafficking between TGN and recycling endosomes in polarized epithelial cells. *J. Cell Biol.* 182:845–853. http://dx.doi.org/10.1083/jcb.200802176

Ohno, H., T. Tomemori, F. Nakatsu, Y. Okazaki, R.C. Aguilar, H. Foelsch, I. Mellman, T. Saito, T. Shirasawa, and J.S. Bonifacino. 1999. Mu1B, a novel adaptor medium chain expressed in polarized epithelial cells. *FEBS Lett.* 449:215–220. http://dx.doi.org/10.1016/S0014-5793(99)00432-9

Palacios, F., L. Price, J. Schweitzer, J.G. Collard, and C. D'Souza-Schorey. 2001. An essential role for ARF6-regulated membrane traffic in adherens junction turnover and epithelial cell migration. *EMBO J.* 20:4973–4986. http://dx.doi.org/10.1093/emboj/20.17.4973

Paris, S., S. Béraud-Dufour, S. Robineau, J. Bigay, B. Antonny, M. Chabre, and P. Chardin. 1997. Role of protein-phospholipid interactions in the activation of ARF1 by the guanine nucleotide exchange factor Arno. *J. Biol. Chem.* 272:22221–22226. http://dx.doi.org/10.1074/jbc.272.35.22221

Prigent, M., T. Dubois, G. Raposo, V. Derrien, D. Tenza, C. Rossé, J. Camonis, and P. Chavrier. 2003. ARF6 controls post-endocytic recycling through its downstream exocyst complex effector. *J. Cell Biol.* 163:1111–1121. http://dx.doi.org/10.1083/jcb.200305029

Rodriguez-Boulan, E., G. Kreitzer, and A. Müsch. 2005. Organization of vesicular trafficking in epithelia. *Nat. Rev. Mol. Cell Biol.* 6:233–247. http://dx.doi.org/10.1038/nrm1593

Salmon, P., and D. Trono. 2006. Production and titration of lentiviral vectors. *Curr. Protoc. Neurosci.* Chapter 4:Unit 4.21. http://dx.doi.org/10.1002/0471142301.ns0421s37

Santy, L.C., and J.E. Casanova. 2001. Activation of ARF6 by ARNO stimulates epithelial cell migration through downstream activation of both Rac1 and phospholipase D. *J. Cell Biol.* 154:599–610. http://dx.doi.org/10.1083/jcb.200104019

Scales, S.J., R. Pepperkok, and T.E. Kreis. 1997. Visualization of ER-to-Golgi transport in living cells reveals a sequential mode of action for COPII and COPI. *Cell.* 90:1137–1148. http://dx.doi.org/10.1016/S0092-8674(00)80379-7

Sheff, D.R., E.A. Daro, M. Hull, and I. Mellman. 1999. The receptor recycling pathway contains two distinct populations of early endosomes with different sorting functions. *J. Cell Biol.* 145:123–139. http://dx.doi.org/10.1083/jcb.145.1.123

Song, J., Z. Khachikian, H. Radhakrishna, and J.G. Donaldson. 1998. Localization of endogenous ARF6 to sites of cortical actin rearrangement and involvement of ARF6 in cell spreading. *J. Cell Sci.* 111:2257–2267.

Vitale, N., J. Mawet, J. Camonis, R. Regazzi, M.F. Bader, and S. Chasserot-Golaz. 2005. The Small GTPase RalA controls exocytosis of large dense core secretory granules by interacting with ARF6-dependent phospholipase D1. *J. Biol. Chem.* 280:29921–29928. http://dx.doi.org/10.1074/jbc.M413748200

Volpicelli-Daley, L.A., Y. Li, C.J. Zhang, and R.A. Kahn. 2005. Isoform-selective effects of the depletion of ADP-ribosylation factors 1-5 on membrane traffic. *Mol. Biol. Cell.* 16:4495–4508. http://dx.doi.org/10.1091/mbc.E04-12-1042

Wang, Y.J., J. Wang, H.Q. Sun, M. Martinez, Y.X. Sun, E. Macia, T. Kirchhausen, J.P. Albanesi, M.G. Roth, and H.L. Yin. 2003. Phosphatidylinositol 4 phosphate regulates targeting of clathrin adaptor AP-1 complexes to the Golgi. *Cell.* 114:299–310. http://dx.doi.org/10.1016/S0092-8674(03)00603-2

Wolff, N.A., W.K. Lee, M. Abouhamed, and F. Thévenod. 2008. Role of ARF6 in internalization of metal-binding proteins, metallothionein and transferrin, and cadmium-metallothionein toxicity in kidney proximal tubule cells. *Toxicol. Appl. Pharmacol.* 230:78–85. http://dx.doi.org/10.1016/j.taap.2008.02.008

Yang, C.Z., and M. Mueckler. 1999. ADP-ribosylation factor 6 (ARF6) defines two insulin-regulated secretory pathways in adipocytes. *J. Biol. Chem.* 274:25297–25300. http://dx.doi.org/10.1074/jbc.274.36.25297